# General Disclaimer

One or more of the Following Statements may affect this Document

- This document has been reproduced from the best copy furnished by the organizational source. It is being released in the interest of making available as much information as possible.

- This document may contain data, which exceeds the sheet parameters. It was furnished in this condition by the organizational source and is the best copy available.

- This document may contain tone-on-tone or color graphs, charts and/or pictures, which have been reproduced in black and white.

- This document is paginated as submitted by the original source.

- Portions of this document are not fully legible due to the historical nature of some of the material. However, it is the best reproduction available from the original submission.
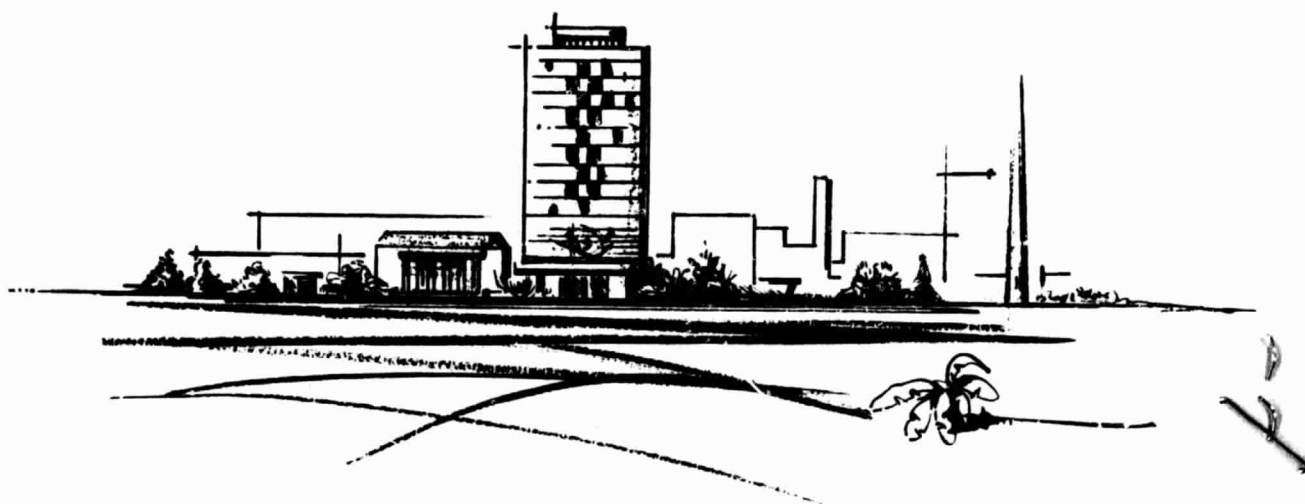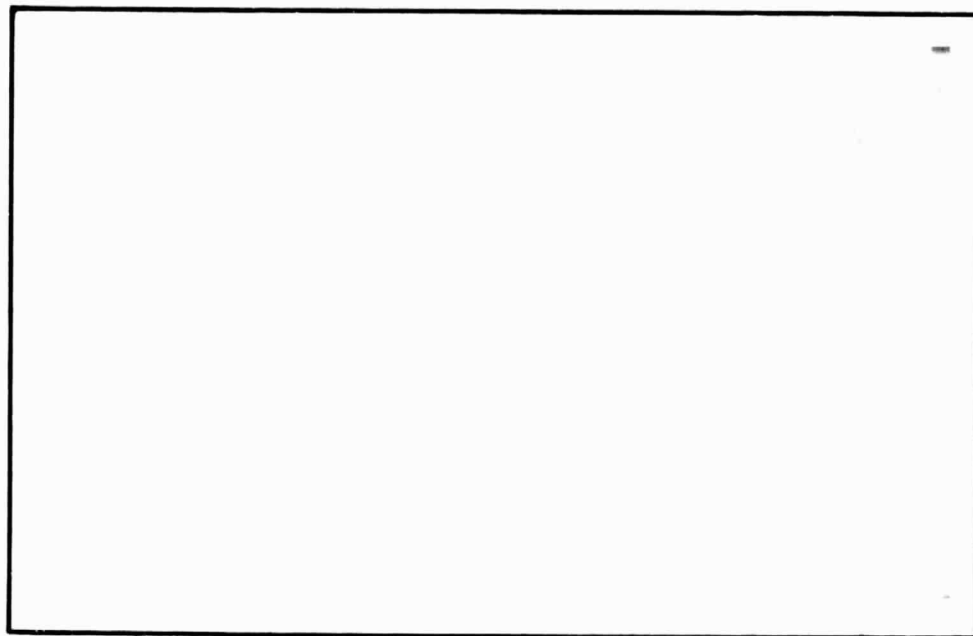
Produced by the NASA Center for Aerospace Information (CASI)

RESEARCH REPORT

BATTELLE MEMORIAL INSTITUTE

COLUMBUS LABORATORIES

BATTELLE MEMORIAL INSTITUTE

COLUMBUS LABORATORIES ● 505 KING AVENUE ● COLUMBUS, OHIO 43201

DEDICATED TO THE ADVANCEMENT OF SCIENCE

FIELDS OF RESEARCH

Aeronautics — Astronautics
Agricultural Chemistry
Agricultural Economics
Alloy Development
Applied Mathematics
Area Economics
Biochemistry
Biophysics — Bionics
Catalysis -- Surface Chemistry
Ceramics
Chemical Engineering
Chemical Processes
Communications Science
Computer Technology
Corrosion Technology
Earth — Atmospheric Sciences
Electrochemistry
Electronics
Energy Conversion
Engineering — Structural Materials
Environmental Systems
Extractive Metallurgy
Extreme-Temperature Technology
Ferrous Metallurgy
Food Technology

Foundry Practice
Fuels — Combustion
Glass Technology
Graphic Arts Technology
Immunology — Cancer Studies
Industrial Economics
Industrial Physics
Information Research
Inorganic Chemistry
Instrumentation
Light Alloys — Rare Metals
Lubricant Technology
Materials Separation — Concentration
Mechanical Engineering
Metal Fabrication Engineering
Metal Finishing
Metallurgical Processes
Microbiology
Microscopy — Mineralogy
Nondestructive Evaluation Technology
Nonferrous Metallurgy
Nucleonics
Ocean Engineering
Organic Chemistry

Organic Coatings
Packaging Research
Particle Dynamics
Petrochemicals
Petroleum Engineering
Pharmaceutical Chemistry
Physical Chemistry
Production Engineering
Psychological Sciences
Pulp — Paper Technology
Radioisotopes — Radiation
Reactor Technology
Refractories
Reliability Engineering
Rubber — Plastics
Semiconductors — Solid-State Devices
Sound — Vibration
Systems Engineering
Textiles — Fibers
Theoretical — Applied Mechanics
Thermodynamics
Transportation
Welding — Metals-Joining Technology
Wood — Forest Products

ANNUAL SUMMARY REPORT
(May 1, 1967, through April 30, 1968)

on

THE EFFECT OF COMPOSITION ON THE
MECHANISM OF STRESS-CORROSION CRACKING
OF TITANIUM ALLOYS IN N_2O_4, AND
AQUEOUS AND HOT-SALT ENVIRONMENTS

to

NATIONAL AERONAUTICS AND SPACE
ADMINISTRATION
Contract No. NASr-100(09)

January 13, 1969

by

J. D. Boyd, F. H. Haynie, P. J. Moreland, W. K. Boyd,
R. A. Wood, D. N. Williams, and R. I. Jaffee

BATTELLE MEMORIAL INSTITUTE
Columbus Laboratories
505 King Avenue
Columbus, Ohio 43201

Battelle Memorial Institute · COLUMBUS LABORATORIES

505 KING AVENUE COLUMBUS, OHIO 43201 · AREA CODE 614, TELEPHONE 299-3151 · CABLE ADDRESS: BATMIN

January 13, 1969

National Aeronautics and Space Administration
Office of Research Grants and Contracts
Office of Space Sciences
600 Independence Boulevard
Washington, D. C. 20546

Attention Mr. T. L. K. Smull
Code RU

Dear Mr. Smull:

> "The Effect of Composition on the Mechanism of
> Stress-Corrosion Cracking of Titanium Alloys in
> N_2O_4, and Aqueous and Hot Salt Environments"
> Contract No. NASr-100(09)

Enclosed are 25 copies of the Annual Summary Report on work performed under the above contract.

Copies of the report have been sent directly to the individuals named in the attached distribution list, deleting names already on the Battelle distribution list.

Yours very truly,

Robert I. Jaffee
Project Coordinator

RIJ:pa
Enc. (25)

cc: Mr. R. H. Raring

TABLE OF CONTENTS

THE EFFECT OF COMPOSITION ON THE MECHANISM OF STRESS-CORROSION CRACKING OF TITANIUM ALLOYS IN N_2O_4, AND AQUEOUS AND HOT-SALT ENVIRONMENTS

by

J. D. Boyd, F. H. Haynie, P. J. Moreland, W. K. Boyd,
R. A. Wood, D. N. Williams, and R. I. Jaffee

SUMMARY

During the 12-month period ending April 30, 1968, considerable progress was made towards understanding the stress-corrosion behavior of titanium alloys in aqueous, hot-salt, and N_2O_4 environments. Some alloys were also evaluated for susceptibility to cracking in methanol. This report summarizes the important results to date, and discusses possible mechanisms of stress-corrosion cracking. The details of the experiments and all the data can be found in previous quarterly reports.

This report is divided into two main sections entitled (1) Testing of Experimental Alloys and (2) Mechanisms of Stress-Corrosion Cracking. The first is a summary of results of the mechanical tests that have been performed on the experimental alloys. These include room-temperature tensile and aqueous stress-corrosion tests, high-temperature creep tests in air and salt environments, and bend tests in N_2O_4. The alloys are rated for susceptibility to stress-corrosion cracking in these environments, and the susceptibility of each is correlated with composition. The second consists of a description of the experiments that have been performed to identify the mechanism of stress-corrosion cracking in aqueous salt solutions, N_2O_4, and methanol. A wide variety of tests and experimental techniques have been employed in this part of the program. These include transmission electron microscopy, scanning electron fractography, crack-velocity measurements, mechanical tests, hydrogen-charging experiments, and radioactive-tracer techniques. The implications of the results of these experiments with regard to possible mechanisms of stress-corrosion cracking are discussed.

TESTING OF EXPERIMENTAL ALLOYS

Materials and Specimen Preparation

The 20 experimental and 2 commercial alloys that were studied are listed in Table 1. The appropriate specimens for each type of test were prepared as described previously, and all specimens were heat treated to have similar microstructures. The α and α/β alloys were stabilized in vacuum for approximately 6 hours at 1200 F, followed by an argon quench. The β alloys were stabilized in air for 1 hour at 1200 F and air quenched. Representative microstructures for two alloys are shown in Figure 1.

TABLE 1. NOMINAL COMPOSITIONS OF ALLOYS

Alloy	Nominal Composition, weight percent
67	Ti-4Al
68	Ti-4Al-4Mo
69	Ti-4Al-4V
70	Ti-4Al-3Mo-1V
41	Ti-4Al-3Mo-1V[a]
71	Ti-4Al-2Mo-2V
72	Ti-4Al-1.5Mo-0.5V
73	Ti-8Al
74	Ti-8Al-3Mo-1V
75	Ti-8Al-3Mo-1V
21	Ti-8Al-2Mo
76	Ti-8Al-2V
77	Ti-8Al-1.5Mo-0.5V
78	Ti-8Al-1Mo-1V
81	Ti-8Al-1Mo-1V[a]
1	Ti-24V
2	Ti-12Mo-12V
3	Ti-18Mo-6V
4	Ti-24Mo
5	Ti-3Al-12Mo-12V
6	Ti-3Al-18Mo-6V
7	Ti-3Al-24Mo

(a) Commercial mill product.

Tensile Tests

The base-line room-temperature tensile data for α and α/β alloys are given in Table 2. Transverse samples (with respect to the final rolling direction) were tested for all materials, and longitudinal samples were tested for a few compositions. Directionality was found although it does not appear too severe. Tensile yield strengths are commensurate with total beta-stabilizer content; Ti-8Al base alloys generally are at a higher strength level than are Ti-4Al base alloys.

Ti-4Al Base		Ti-8Al Base	
Avg Yield Strength, ksi	β Content, percent	Avg Yield Strength, ksi	β Content, percent
67	0	100	0
102	1.5Mo-0.5V	119	1Mo
106	4V	119	2V
108	2Mo-2V	131	1.5Mo-0.5V
110	4Mo	133	1Mo-1V (commercial)
114	3Mo-1V	136	1Mo-1V
122	3Mo-1V (commercial)	138	2Mo
		141	3Mo-1V
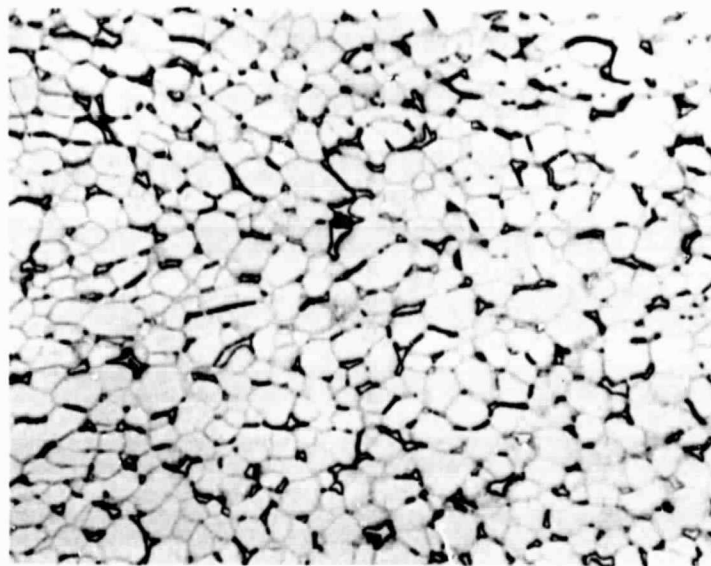
500X   2C850
a.   Alloy 78, Ti-8Al-1Mo-1V
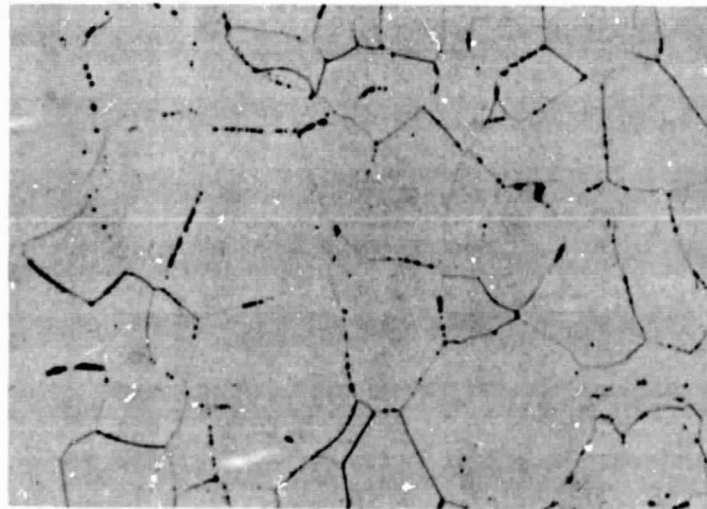
150X   1D306
b.   Alloy 2, Ti-12Mo-12V

FIGURE 1.   TYPICAL MICROSTRUCTURES OF ANNEALED
α/β AND β ALLOYS

TABLE 2. ROOM-TEMPERATURE TENSILE DATA

Alloy	Composition, percent	Test Direction[a]	0.2% Offset Yield Strength, ksi	Ultimate Strength, ksi	Ductility, percent Elongation	Reduction in Area
67	Ti-4Al	L	65	80	23	42
		L	69	81	23	44
		T	67	79	23	42
		T	67	79	22	41
68	Ti-4Al-4Mo	L	92	111	18	34
		L	91	110	17	30
		T	114	120	18	44
		T	107	113	18	45
69	Ti-4Al-4V	L	93	109	18	21
		L	97	112	21	42
		T	105	112	19	41
		T	108	112	20	43
70	Ti-4Al-3Mo-1V	L	93	114	17	28
		L	93	111	17	35
		T	114	119	18	47
		T	115	119	15	46
41	Ti-4Al-3Mo-1V (commercial)	T	121	128	17	39
		T	123	130	18	40
71	Ti-4Al-2Mo-2V	T	109	113	17	43
		T	108	112	19	45
72	Ti-4Al-1.5Mo-0.5V	T	101	107	21	34
		T	104	108	13	38
73	Ti-8Al	T	101	102	26	33
		T	99	100	25	40
74	Ti-8Al-3Mo-1V	T	140	157	20	26
		T	141	159	20	22
75	Ti-8Al-1Mo	T	119	125	20	25
		T	119	124	19	34
21	Ti-8Al-2Mo	T	139	150	18	22
		T	138	154	17	25
76	Ti-8Al-2V	T	118	127	13	21
		T	119	127	13	22
77	Ti-8Al-1.5Mo-0.5V	T	130	146	17	28
		T	131	147	19	29
78	Ti-8Al-1Mo-1V	L	129	147	15	22
		L	129	143	17	23
		T	138	151	15	16
		T	133	147	17	26
81	Ti-8Al-1Mo-1V (commercial)	T	131	145	20	26
		T	134	147	18	21

(a) L = longitudinal
   T = transverse.

TABLE 3. STRAIN-RATE-SENSITIVITY DATA

Specification	Alloy	Test Direction	$\partial(\log \sigma)/\partial(\log \dot{\epsilon})$
67-1	Ti-4Al	T	0.0191
67-9		T	0.0183
67-13		L	0.0207
67-16		L	0.0199
68-1	Ti-4Al-4Mo	T	0.0170
68-3		T	0.0157
68-16		L	0.0178
68-13		L	0.0187
69-1	Ti-4Al-4V	T	0.0161
69-9		T	0.0157
69-21		L	0.0327
69-19		L	0.0161
70-9	Ti-4Al-3Mo-1V	T	0.0157
70-2		T	0.0140
70-10		T	0.0128
70-16		L	0.0187
70-13		L	0.0195
71-9	Ti-4Al-2Mo-2V	T	0.0149
71-2		T	0.0145
72-2	Ti-4Al-1.5Mo-0.5V	T	0.0157
72-7		T	0.0157
73-7	Ti-8Al	T	0.0178
73-1		T	0.0161
74-1	Ti-8Al-3Mo-1V	T	0.0111
74-5		T	0.0098
75-1	Ti-8Al-1Mo	T	0.0132
75-5		T	0.0111
76-1	Ti-8Al-2V	T	0.0136
76-8		T	0.0132
77-1	Ti-8Al-1.5Mo-0.5V	T	0.0115
77-8		T	0.0128
78-1	Ti-8Al-1Mo-1V	T	0.0128
78-15		L	0.0132
78-11		L	0.0132
21-1	Ti-8Al-2Mo	T	0.0119
21-8		T	0.0124
41-8	Ti-4Al-3Mo-1V	T	0.0145
41-1	(commercial)	T	0.0149
81-2	Ti-8Al-1Mo-1V	T	0.0128
81-6	(commercial)	T	0.0145

Acceptable ductility was found in all compositions, with better ductilities being exhibited by Ti-4Al base alloys than by Ti-8Al base alloys. However, within each group, composition-ductility relationships are not consistent with composition-strength relationships. The good ductilities of the alloys having 3 percent molybdenum plus 1 percent vanadium beta-stabilizer content are noted.

The strain-rate sensitivity of each of the experimental alloys was estimated from the change in stress accompanying the change in strain rate during tensile testing. The strain-rate-sensitivity parameter, $\partial(\log \sigma)/\partial(\log \dot{\epsilon})$, for each alloy is given in Table 3. The binary alloys, Ti-4Al and Ti-8Al, are the most sensitive to strain-rate changes. Of the α-β alloys, the Ti-8Al-base alloys appear to have a strain-rate sensitivity lower than that of the Ti-4Al-base alloys.

Longitudinal samples of the beta alloys were tensile tested at room temperature. These data are given in Table 4. Longitudinal samples were examined instead of transverse samples owing to size limitations of the sheets produced. However, as single-phase alloys, the longitudinal properties should differ little from transverse properties. The data show the generally low-strength, high-ductility characteristics expected of highly alloyed beta compositions. The best ductility was found for the highest strength alloy, Ti-3Al-18Mo-6V. However, there does not appear to be a consistent relationship between ductility and strength level among the beta compositions examined.

TABLE 4. ROOM-TEMPERATURE TENSILE PROPERTIES OF LONGITUDINAL SAMPLES OF BETA ALLOYS IN THE SOLUTION-ANNEALED AND STABILIZED CONDITION

Alloy	Composition, percent (Balance Ti)	0.2% Offset Yield Strength, ksi	Ultimate Strength, ksi	Ductility, percent	
				Elongation	Reduction in Area
1	24V	84	94	16	32
2	12Mo-12V	102	109	13	31
3	18Mo-6V	106	112	15	42
4	24Mo	107	113	16	36
5	3Al-12Mo-12V	106	111	12	22
6	3Al-18Mo-6V	111	116	17	45
7	3Al-24Mo	109	114	12	16

Aqueous Stress-Corrosion Tests

The precracked-cantilever test was employed to determine the fracture-toughness parameters of the various alloys in air and 3.5 percent NaCl solution. The critical stress intensities to produce accelerated crack growth in each environment were determined. Table 5 summarizes the data for transverse samples of the α and α/β alloy series.

TABLE 5. FRACTURE-TOUGHNESS DATA FOR ALPHA AND ALPHA-BETA ALLOYS OBTAINED
IN AIR AND 3.5 PERCENT NaCl SOLUTION ENVIRONMENTS (STEP-LOADED AND
CONSTANT LOAD TESTS ON TRANSVERSE SAMPLES)

Alloy	Composition, percent (Balance Ti)	Environment	Loading Method	Stress Intensity, ksi $\sqrt{inch}$	Total Exposure Time, minutes	Remarks
67	4 Al	Air	Step	>68.2	~140	Twist, no failure
		Air	Ditto	>102.3	~140	Ditto
		Salt water	"	>77.4	~130	"
		Salt water	"	>76.8	~73	"
		Air[a]	"	85.7	~140	Failed
		Salt water[a]	"	83.3	~140	Failed
		Salt water[a]	Constant	83.1	3	Failed
		Salt water[a]	Constant	80.2	360	No failure
68	4Al-4Mo	Air	Step	92.9	111	Failed
		Salt water	Step	87.6	106	Ditto
		Salt water	Constant	86.3	182	"
		Salt water	Constant	85.0	360	No failure
69	4Al-4V	Air	Step	88.5	154	Failed
		Salt water	Ditto	98.6[b]	185	Ditto
		Salt water	"	88.2	99	"
		Salt water	Constant	96.7	0.1	"
		Salt water	Ditto	88.7	6	"
		Salt water	"	84.1	360	No failure
70	4Al-3Mo-1V	Air	Step	94.9	187	Failed
		Salt water	Step	92.8	173	Ditto
		Salt water	Constant	89.3	12	"
		Salt water	Ditto	77.6	360	No failure
		Salt water	"	85.2	360	Ditto
		Salt water	"	87.2	360	"
41	4Al-3Mo-1V (commercial)	Air	Step	92.8	67	Failed
		Salt water	Step	89.8	65	Ditto
		Salt water	Constant	87.8	228	"
		Salt water	Constant	84.2	360	No failure
71	4Al-2Mo-2V	Air	Step	94.4	86	Failed
		Salt water	Step	92.2	68	Ditto
		Salt water	Constant	89.8	94	"
		Salt water	Constant	86.5	360	No failure
72	4Al-1.5Mo-0.5V	Air	Step	91.7	102	Failed
		Salt water	Step	90.4	86	Ditto
		Salt water	Constant	83.9	5	"
		Salt water	Constant	82.9	360	No failure
73	8Al	Air	Step	96.5	166	Failed
		Salt water	Step	26.5	29	Ditto
		Salt water	Constant	30.7	10	"
		Salt water	Ditto	26.1[c]	360[c]	No failure[b]
		Salt water	"	25.6	360	Ditto
		Salt water	Step	33.6[b]	78[b]	Failed[c]

TABLE 5. (Continued)

Alloy	Composition, percent (Balance Ti)	Environment	Loading Method	Stress Intensity, ksi $\sqrt{inch}$	Total Exposure Time, minutes	Remarks
74	8Al-3Mo-1V	Air	Step	54.9	101	Failed
		Salt water	Step	13.3	17	Ditto
		Salt water	Constant	15.6	3	"
		Salt water	Constant	12.5	360	No failure
75	8Al-1Mo	Air	Step	68.7	150	Failed
		Salt water	Step	19.4	22	Ditto
		Salt water	Constant	28.0	4	"
		Salt water	Ditto	17.5	360	No failure
		Salt water	"	19.2[c]	360[c]	Ditto[c]
		Salt water	Step	30.5[d]	98[d]	Failed[d]
21	8Al-2Mo	Air	Step	64.9	64	Ditto
		Salt water	Step	22.6	26	"
		Salt water	Constant	21.9	3	"
		Salt water	Constant	20.8	360	No failure
76	8Al-2V	Air	Step	101.6	117	Failed
		Salt water	Step	24.6	24	Ditto
		Salt water	Constant	24.1	4	"
		Salt water	Constant	23.4	360	No failure
77	8Al-1.5Mo-0.5V	Air	Step	78.8	75	Failed
		Salt water	Step	16.9	2	Ditto
		Salt water	Constant	15.7	22	"
		Salt water	Constant	14.6	360	No failure
78	8Al-1Mo-1V	Air	Step	64.4	101	Failed
		Salt water	Step	25.0	44	Ditto
		Salt water	Constant	24.3	23	"
		Salt water	Ditto	22.3	360	No failure
		Salt water	"	23.6	360	Ditto
81	8Al-1Mo-1V (commercial)	Air	Step	90.3	104	Failed
		Salt water	Step	19.0	17	Ditto
		Salt water	Constant	24.4	1	"
		Salt water	Constant	19.0	360	No failure

(a) 1/4-inch-thick samples. All other data are for 1/8-inch-thick samples.
(b) Believed to be anonomously high.
(c) Sample not failing in 360 minutes was subsequently step-loaded to failure.
(d) Sample step-loaded to failure after 360-minute exposure shown [Footnote (c)].

An analysis of the Table 5 data shows that the toughness in air of the Ti-4Al base alloys is greater than that of the Ti-8Al base alloys. The ranking of compositions in order of decreasing toughness in air as shown below indicates no particular correlation with amount or kind of beta-stabilizer addition.

Ranking According to Toughness in Air

	Ti-4Al Base			Ti-8Al Base	
Alloy	β-Stabilizing Content, percent	Stress Intensity for Air Failure, ksi $\sqrt{inch}$	Alloy	β-Stabilizing Content, percent	Stress Intensity for Air Failure, ksi $\sqrt{inch}$
67	0	>100	76	2V	102
70	3Mo-1V	95	73	0	96
71	2Mo-2V	94	81	1Mo-1V[b]	90
68	4Mo	93	77	1.5Mo-0.5V	79
41	3Mo-1V[b]	93	75	1Mo	69
72	1.5Mo-0.5V	92	21	2Mo	65
69	4V	88	78	1Mo-1V	64
67[a]	0	86	74	3Mo-1V	55

(a) 1/4 inch thick.
(b) Commercial material.

The toughness of the Ti-4Al-base alloys in salt water is markedly greater than that of the Ti-8Al-base alloys. The ranking of compositions in order of decreasing toughness in salt water is shown below (for constant load tests).

Ranking According to Toughness in Salt Water, Stress Intensity

	Ti-4Al Base				Ti-8Al Base		
	β-Stabilizing Content, percent	Stress Intensity in Salt Water, ksi $\sqrt{inch}$			β-Stabilizing Content, percent	Stress Intensity in Salt Water, ksi $\sqrt{inch}$	
Alloy		For No Failure[a]	For Failure	Alloy		For No Failure[a]	For Failure
67	0	>77	(b)	73	0	26	31
70	3Mo-1V	87	89	78	1Mo-1V	24⁻	24⁺
71	2Mo-2V	86	90	76	2V	23	24
68	4Mo	85	86	21	2Mo	21	22
41	3Mo-1V[c]	84	88	75	1Mo	19	24
69	4V	84	89	81	1Mo-1V[c]	19	24
72	1.5Mo-0.5V	83	84	77	1.5Mo-0.5V	15	16
67[d]	0	80	83	74	0	12	16

(a) In 360 minutes (test then discontinued).
(b) Extremely tough. Stress-intensity values not determined owing to twisting of samples.
(c) Commercial material
(d) 1/4-in.-thick material.

Again, no correlation of toughness with amount or kind of beta-stabilizer addition is apparent. However, the possible relationship between large beta-stabilizer addition and good toughness is observed for Ti-4Al-base alpha-beta alloys. Such relationship is reversed for alloys having a Ti-8Al base.

The ranking of susceptibility of the alloys in this series to accelerated crack growth in salt water (least to most susceptible, based on salt-water-stress intensity/air-stress-intensity ratio) is shown below using the Table 5 data.

Ranking According to Toughness in Salt Water, percent

| | Ti-4Al Base | | | | Ti-8Al Base | | |
| | | Stress-Intensity Ratio (SW/A), % | | | | Stress-Intensity Ratio (SW/A), % | |
Alloy	β-Stabilizing Content, percent	(a)	(b)	Alloy	β-Stabilizing Content, percent	(a)	(b)
67[d]	0	100	100	78	1Mo-1V	38	39
69[d]	4V	96	100	21	2Mo	32	35
67[d]	0	93	96	75	1Mo	28	28
70	3Mo-1V	92	98	73	0	27	27
71	2Mo-2V	92	98	76	2V	23	24
68	4Mo	91	95	74	3Mo-1V	22	24
41	3Mo-1V[c]	90	97	81	1Mo-1V[c]	21	21
72	1.5Mo-0.5V	90	98	77	1.5Mo-0.5V	19	22

(a) Based on constant-load seawater tests.
(b) Based on incremental-load seawater tests.
(c) Commercial material.
(d) 1/4-inch-thick material.

It is apparent that the Ti-4Al-base alloys are not susceptible, while the Ti-8Al-base alloys are very susceptible. No significant trends for the effect of the amount and kind of beta-stabilizer addition on the two bases are observed when susceptibility ratios are compared. Apparently, the composition of the α phase largely determines the susceptibility of these alloys, probably through the $\alpha \rightarrow \alpha_2$ ordering reaction. A series of borderline Ti-7Al-base alloys is presently being studied in an attempt to demonstrate the effect of beta-stabilizing elements. Preliminary tests have shown that this aluminum content produces marginal susceptibility, and is therefore the most likely to be affected by other variables.

Two special tests were run to clarify the following points: (1) the necessity of a preexisting fatigue crack in defining critical-stress-intensity values and (2) the effects of an additional thermal exposure in the temperature range which promotes the $\alpha \rightarrow \alpha + \alpha_2$ transformation. It was found that samples without fatigue cracks are not as readily susceptible to cracking as fatigue-cracked samples. For example:

Alloy 70, Ti-4Al-3Mo-1V

Salt water, constant load, fatigue cracked: 89.3 ksi $\sqrt{\text{inch}}$ (failed)

Salt water, constant load, saw cut only: 89.3 ksi $\sqrt{\text{inch}}$ (no failure)

Alloy 78, Ti-8Al-1Mo-1V

Salt water, constant load, fatigue cracked: 24.3 ksi $\sqrt{inch}$ (failed)

Salt water, constant load, saw cut only: 24.3 ksi $\sqrt{inch}$ (no failure)

Salt water, step loaded, fatigue cracked: 25.0 ksi $\sqrt{inch}$ (failed)

Salt water, step loaded, saw cut only: 60.2 ksi $\sqrt{inch}$ (failed).

One sample, prepared and annealed in the standard way, was additionally exposed in argon for 24 hours at 1112 F plus 24 hours at 1022 F and air cooled. The step-loaded test conducted with this sample resulted in a failure at a very low stress-intensity value as shown below.

Alloy 78, Ti-8Al-1Mo-1V

Salt water, step loaded, fatigue cracked: 25.0 ksi $\sqrt{inch}$ (failed)

Thermally exposed, salt water, step loaded, fatigue cracked:
17.1 ksi $\sqrt{inch}$ (failed).

This result indicates that the standard annealing treatment given all samples may not be the most sensitive condition. Further testing is planned to evaluate the effect.

The toughness of the beta alloys was determined on longitudinal samples, using the incremental-loading technique in both air and salt water. The data are given in Table 6. All of the alloys were tough in air and only two alloys, Ti-18Mo-6V and

TABLE 6. FRACTURE-TOUGHNESS DATA FOR BETA ALLOYS OBTAINED IN AIR AND
3.5 PERCENT NaCl SOLUTION ENVIRONMENTS (STEP-LOADED TESTS
ON LONGITUDINAL SAMPLES)

Alloy	Composition, percent (Balance Ti)	Environment	Stress Intensity to Produce Failure, ksi $\sqrt{inch}$		SW/A, percent
1	24V	Air	80.3		101
		Salt water		81.4	
2	12Mo-12V	Air	87.4		100
		Salt water		86.8	
3	18Mo-6V	Air	80.2		66
		Salt water		53.0	
4	24Mo	Air	80.5		94
		Salt water		75.0	
5	3Al-12Mo-12V	Air	87.4		100
		Salt water		86.6	
6	3Al-18Mo-6V	Air	89.6		86
		Salt water		77.2	
7	3Al-24Mo	Air	81.0		75
		Salt water		60.9	

Ti-3Al-24Mo, showed a moderate detrimental effect of salt-water environment on toughness. The possible trend of decreasing toughness (in both air and salt water) and increasing susceptibility with increasing molybdenum content is to be noted. The high toughness obtained for Alloy 4, Ti-24Mo, is anomalous to this trend. Additional work with this series of compositions is planned.

Creep Tests

One sample from each alloy was creep tested using a step-loaded schedule, nominally 24 hours per step. The creep load was increased incrementally until the total plastic strain (load-off measurements) was in the range 0.2 to 1.0 percent. Duplicate samples from these alloys were exposed in 600 F creep stations at essentially constant loads designed to give between 0.2 and 1.0 percent plastic strain in 70 to 100 hours. However, the initial stress levels selected were in some cases inadequate to produce this amount of strain. Thus, selected samples were exposed to increasing stress levels. The data obtained in these tests are given in Table 7. Portions of the creep data obtained on initial samples (step loaded) and the creep exposure data for salt-coated samples also are given in Table 7. Based on all the 600 F creep data generated, the stress levels required to produce between 0.2 and 1.0 percent plastic-creep deformation in about 70 hours are shown below in relation to alloy content and ranked in order of increasing strength. The beneficial elevated-temperature strengthening effect of molybdenum is apparent.

Ranking According to 600 F Creep Strengths

Ti-4Al Base		Ti-8Al Base	
600 F Creep Stress, ksi	β-Stabilizing Content, percent	600 F Creep Stress, ksi	β-Stabilizing Content, percent
32	0	59	0
64	4V	79	1Mo
64.5	1.5Mo-0.5V	85	2V
73	3Mo-1V	90	1Mo-1V (commercial)
73.5	2Mo-2V	94	1.5Mo-0.5V
74	4V	95	1Mo-1V
84.5	3Mo-1V (commercial)	98	2Mo
		110	3Mo-1V

Samples were tested in tension at room temperature after creep exposure. None of the alloys were found to be unstable after the 600 F creep exposures. Instability is defined as at least a 50 percent reduction in one or more of the tensile-ductility measurements.

Hot-Salt Stress-Corrosion Results

A similar 72-hour, 600 F creep exposure of samples coated with a salt (NaCl) slurry constituted the hot-salt stress-corrosion exposure. Evaluation of sample surface conditions after exposure and of room-temperature tensile results obtained on exposed samples constituted the hot-salt stress-corrosion test.

TABLE 7. 600 F CREEP DATA OBTAINED ON TRANSVERSE SAMPLES OF ALPHA AND ALPHA-BETA ALLOYS WITH AND WITHOUT SALT COATINGS

Alloy	Composition, percent (Balance Ti)	Sample	Exposure Penultimate		Exposure Ultimate		Total Time, hr	Total Strain, percent	Total Plastic Strain, percent
			Stress, ksi	Time, hr	Stress, ksi	Time, hr			
67	4Al	1	22	24	32	24	48	0.714	0.476
		2	30	24	32	48	73	0.643	0.429
	(Salt coated)	3	32	_(a)	32	72	72	_(b)	_(b)
68	4Al-4Mo	1	70	24	75	24	186	1.200	0.743
		2	72	24	74	53	77	0.757	0.305
	(Salt coated)	3	74	_(a)	74	72	72	_(b)	_(b)
69	4Al-4V	1	55	24	65	24	140	0.776	0.352
		2	62	24	64	48	98	0.681	0.295
	(Salt coated)	3	64	_(a)	64	72	72	_(b)	_(b)
70	4Al-3Mo-1V	1	70	24	75	24	96	0.952	0.476
		2	70	24	72	50	74	0.748	0.305
	(Salt coated)	3	73	_(a)	73	72	72	_(b)	_(b)
41	4Al-3Mo-1V	1	80	65	85	24	139	0.976	0.448
	(Commercial)	2	82	114	84	48	188	0.724	0.219
	(Salt coated)	3	84.5	_(a)	84.5	72	72	_(b)	_(b)
71	4Al-2Mo-2V	1	70	24	75	24	137	0.829	0.390
		2	70	29	72	49	78	0.643	0.219
	(Salt coated)	3	73.5	_(a)	73.5	72	72	_(b)	_(b)
72	4Al-1.5Mo-0.5V	1	60	1.6	65	24	50	0.981	0.548
		2	62	42	64	30	98	0.662	0.267
	(Salt coated)	3	64.5	_(a)	64.5	72	72	_(b)	_(b)
73	8Al	1	55	67	65	0.1	121	_(c)	2.700
		2	58	24	60	49	73	1.52	1.100
	(Salt coated)	3	59	_(a)	59	72	72	_(b)	_(b)
74	8Al-3Mo-1V	1	105	48	107	43	351	0.853	0.205
		2	109	30	110	48	146	0.890	0.238
	(Salt coated)	3	110	_(a)	110	72	72	_(b)	_(b)
75	8Al-1Mo	1	80	48	82	43	328	1.020	0.486
		2	80	_(a)	80	52	52	2.340	1.730
	(Salt coated)	3	79	_(a)	79	72	72	_(b)	_(b)
21	8Al-2Mo	1	95	24	100	0.1	210	_(c)	0.219
		2	97	48	98.5	48	123	1.250	0.614
	(Salt coated)	3	98	_(a)	98	72	72	_(b)	_(b)
76	8Al-2V	1	80	24	85	24	168	0.786	0.214
		2	85	_(a)	85	48	48	0.833	0.271
	(Salt coated)	3	85	_(a)	85	72	72	_(b)	_(b)
77	8Al-1.5Mo.0.5V	1	90	24	95	3.3	75	1.100	0.467
		2	93	_(a)	93	48	48	0.809	0.262
	(Salt coated)	3	94	_(a)	94	72	72	_(b)	_(b)

TABLE 7. (Continued)

| Alloy | Composition, percent (Balance Ti) | Sample | Exposure Penultimate | | Exposure Ultimate | | Total Time, hr | Total Strain, percent | Total Plastic Strain, percent |
			Stress, ksi	Time, hr	Stress, ksi	Time, hr			
78	8Al-1Mo-1V	1	90	24	95	3.2	75	1.000	0.395
		2	95	48	97	66	138	1.16	0.524
	(Salt coated)	3	96	_(a)	96	42	42	_(d)	_(b)
	(Salt coated)	4	95	_(a)	95	41	41	_(d)	_(b)
	(Salt coated)	5	94	_(a)	94	41	41	_(d)	_(b)
81	8Al-1Mo-1V	1	80	24	90	24	72	0.890	0.309
	(Commercial)	2	90	_(a)	90	48	48	0.914	0.357
	(Salt coated)	3	90	_(a)	90	72	72	_(b)	_(b)

(a) Constant-load test. Thus penultimate load same as ultimate load.

(b) Not measured.

(c) Sample began to deform rapidly upon loading, whereupon load was quickly removed.

(d) Sample failed in test at total time indicated and exhibited severe salt stress-corrosion attack.

Following the 600 F exposure of salt-coated samples in the creep stations, the salt coatings were washed off and the samples examined. Hot-salt stress-corrosion cracks were visible on all samples from the Ti-8Al-base alloys. Among the Ti-4Al-base alloys, only the Ti-4Al-3Mo-1V compositions (both experimental and commercial alloys) had salt cracks. The cracks were visible with the unaided eye, with optical magnification, and could be revealed with dye-penetrant inspection technique.

The hot-salt-exposed samples were next tested in a standard room-temperature tensile test to determine residual strength and ductility. The experimental Ti-8Al-1Mo-Ti-8Al-1Mo-1V alloy, Alloy 78, did not survive the creep exposure in three trials, each at a lower stress level than the previous try, so no tensile evaluation was possible. The room-temperature tensile data obtained on salt-exposed samples are given in Table 8. Average base-line tensile data and average unsalted, creep-exposed tensile data are included in this table for comparison purposes. These data reveal, as would be expected, that drastic reductions in mechanical properties, especially ductility parameters, are caused by the stress-corrosion cracks. Little change in tensile properties is found when no stress-corrosion cracks are formed.

At the fracture of samples damaged by hot-salt, stress-corrosion, the depth and extent of the cracks as well as the number of cracks in the fracture plane can be readily determined. Crack surfaces are oxidized during exposure and appear typically as half-moon shaped discolorations (bluish purple) on the otherwise silver-bright fracture surface. The cracks originated most frequently at the edges of the sheet samples. The number of cracks observed on the fracture surfaces of the samples are shown below.

Ranking According to Hot-Salt Cracks

	Ti-4Al Base			Ti-8Al Base	
Alloy	β-Stabilizing Content	Cracks	Alloy	β-Stabilizing Content	Cracks
67	0	0	73	0	2
68	4Mo	0	74	3Mo-1V	4
69	4V	0	75	1Mo	6
70	3Mo-1V	1	21	2Mo	6
41	3Mo-1V (commercial)	3	76	2V	6
71	2Mo-2V	0	77	1.5Mo-0.5V	4
72	1.5Mo-0.5V	0	78	1Mo-1V	Typically 6
			81	1Mo-1V (commercial)	6

Stress-Corrosion Tests in N_2O_4

Fifteen experimental titanium alloys machined into 4 x 0.5 x 0.07-inch sheet specimens have been exposed to "red" N_2O_4 for 30 days at 105 F. The specimens were stressed by constant deflection in stainless steel three-point-loading fixtures. The stress level of each specimen was 90 percent of the 0.2 percent offset yield strength based on assumed values of the modulus of elasticity and previously measured values of the yield strength for each alloy. There were no failures in any of the exposed specimens. The [HNO$_3$]/[H$_2$O] ratio in the N_2O_4 was then changed by the procedure described previously, and specimens of each alloy were tested in the new environment. All of the exposed specimens failed by stress-corrosion cracking. Thus the stress-corrosion cracking of titanium alloys in N_2O_4 is largely dependent on the composition of

TABLE 8. ROOM-TEMPERATURE TENSILE PROPERTIES OF TRANSVERSE SAMPLES OF ALPHA AND ALPHA-BETA ALLOYS

(Average Base-Line Data and Data Obtained After 600 F Creep and Hot-Salt Exposure)

Alloy	Composition, percent (Balance Ti)	0.2% Offset Yield Strength, ksi			Ultimate Strength, ksi			Elongation, percent			Reduction in Area, percent		
		Base Average	Average After Creep	After Hot-Salt Exposure	Base Average	Average After Creep	After Hot-Salt Exposure	Base Average	Average After Creep	After Hot-Salt Exposure	Base Average	Average After Creep	After Hot-Salt Exposure
67	4Al	67	69	70	79	79.5	80.	22.5	22.5	21	41.5	42	42
68	4Al-4Mo	110.5	110.5	113	116.5	121.5	121	18	17	15	44.5	43	31
69	4Al-4V	106.5	111	110	112	124	124	19.5	16	16	42	38	40
70	4Al-3Mo-1V	114.5	112.5	114	119	121.5	121	16.5	16.5	9	46.5	44.5	16
41	4Al-3Mo-1V(b)	122	119	120	129	131	130	17.5	15	9	39.5	37.5	14
71	4Al-2Mo-2V	108.5	112	112	112.5	121	121	18	15	15	44	38.5	46
72	4Al-1.5Mo-0.5V	102.5	99	102	107.5	107.5	108	19.5	18	17	36	42.5	41
73	8Al	100	100.5	98	101	103.5	99	25.5	22.5	7	36.5	39.5	13
74	8Al-3Mo-1V	140.5	143.5	142	158	158.5	143.	20	18.5	2	24	20.5	5
75	8Al-1Mo	119	121.5	108	124.5	128	108	19.5	16	3	29.5	28.5	4
21	8Al-2Mo	138.5	138	124	152	149.5	124	17.5	15	2	23.5	20.5	4
76	8Al-2V	118.5	123	112	127	134	112	13	15	2	21.5	24.5	4

TABLE 8. (Continued)

Alloy	Composition, percent (Balance Ti)	0.2% Offset Yield Strength, ksi			Ultimate Strength, ksi			Elongation, percent			Reduction in Area, percent		
		Base Average	Average After Creep	After Hot-Salt Exposure	Base Average	Average After Creep	After Hot-Salt Exposure	Base Average	Average After Creep	After Hot-Salt Exposure	Base Average	Average After Creep	After Hot-Salt Exposure
77	8Al-1.5Mo-0.5V	130.5	133	130	146.5	148	132	18	16	3	28.5	28.5	7
78	8Al-1Mo-1V	135.5	135	-(a)	149	147	-	16	15.5	-	21	27.5	-
81	8Al-1Mo-1V(b)	132.5	131.5	125	146	144	126	19	18	3	23.5	29	10

(a) Multiple samples failed in hot-salt creep exposure. None survived exposure for tensile testing.
(b) Commercial alloy.

17

the N_2O_4. An effort is being made to manufacture N_2O_4 that produces marginal susceptibility so that the effects of alloy composition can be evaluated.

MECHANISMS OF STRESS-CORROSION CRACKING

Aqueous Environments

The object of this part of the program is to perform the necessary specialized experiments, which, in conjunction with the mechanical tests just described, will provide a broad understanding of the stress-corrosion behavior of titanium alloys in aqueous environments. A mechanism for the aqueous-stress-corrosion cracking of titanium alloys is proposed on the basis of the experimental observations presently available. Additional experiments will be performed during the next year to establish the details of the mechanism.

Fractography

The fracture surfaces of several alloys broken in aqueous-chloride solution have been examined by scanning-electron microscopy, and by electron microscopy of carbon, carbon-platinum replicas. The scanning-electron microscope is especially suitable for fractography because no specimen preparation is required and the depth of field is approximately equal to the field of view at magnifications between 5,000X and 30,000X. A striking difference is observed between specimens broken in salt-water and specimens broken in air. The fracture surfaces of stress-corrosion cracks show many flat, cleavage-like facets (e.g., at A in Figure 2), whereas the fracture surfaces of specimens broken in air exhibit the "dimples" characteristic of ductile fracture (Figure 3). Pairs of stereomicrographs taken by both techniques showed that the flat facets usually lie on the sides of protuberances or depressions. The peaks of the protuberances appear as the bright white lines in the scanning-electron micrographs (Figure 2) and as the dark-black lines in the replicas (e.g., Area C in Figure 4b). Note that the "river-pattern" (Figure 4b) characteristic of cleavage ends abruptly in the vicinity of a grain boundary. These observations suggest that failure originates with cleavage-like cracks in many grains which lead to ductile rupture of the remaining material.

Slip Geometry

The predominant slip systems in the Ti-8Al base alloys are $\{10\bar{1}0\}<1\bar{2}10>$, although there is always some nonprism slip. The slip is confined to straight slip bands spaced approximately 1 micron apart, and there is little cross slip between the slip bands. Consequently, large shears occur in each slip band, which often produce visible steps at grain boundaries (Figure 5a) and large offsets where intragranular β particles are cut (Figure 5b). With decreasing aluminum content, more cross slip is observed. In the Ti-4Al-base alloys, the dislocations are in irregular tangles at low strains, and form a cellular structure at higher strain.
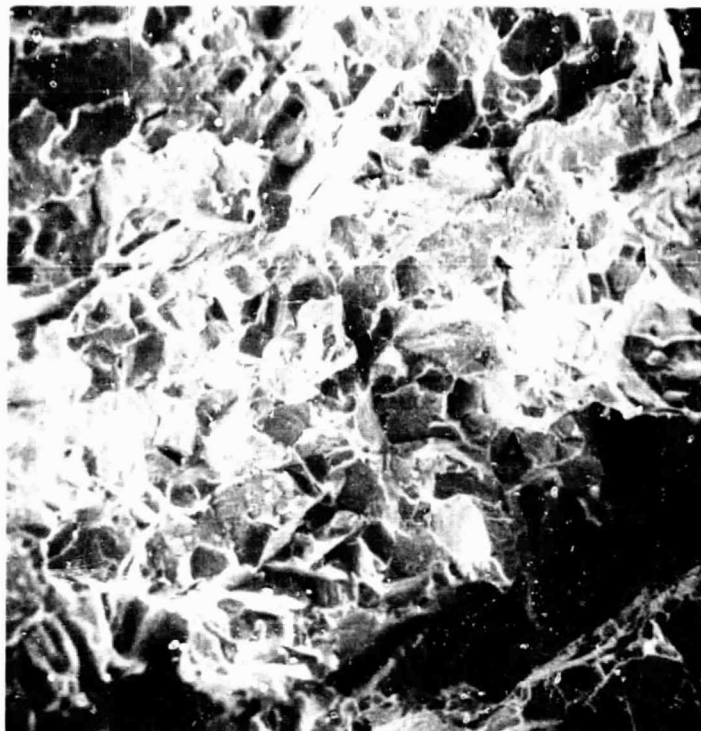
640X

FIGURE 2. SCANNING ELECTRON MICROGRAPH OF A SALT-WATER
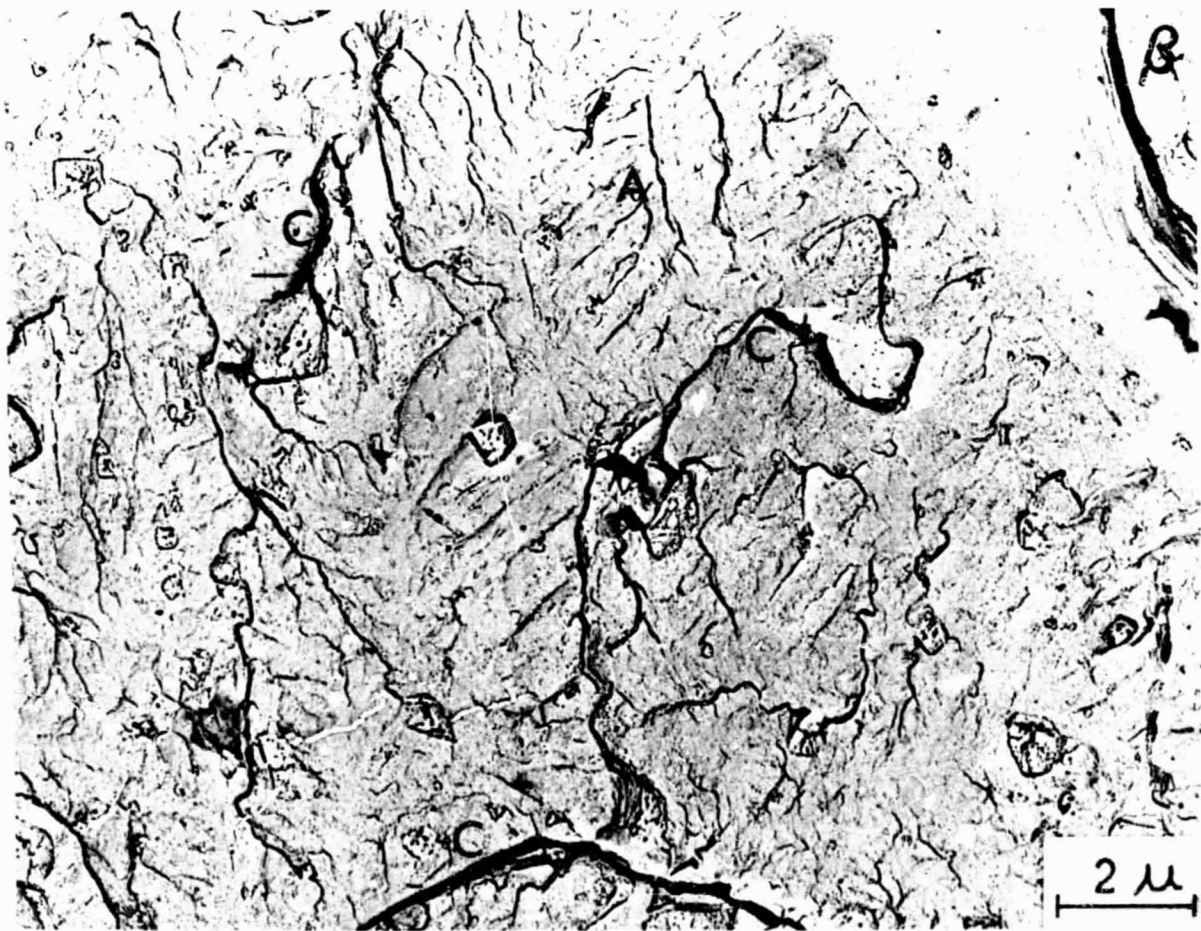STRESS-CORROSION FRACTURE IN Ti-8Al-1Mo-1V
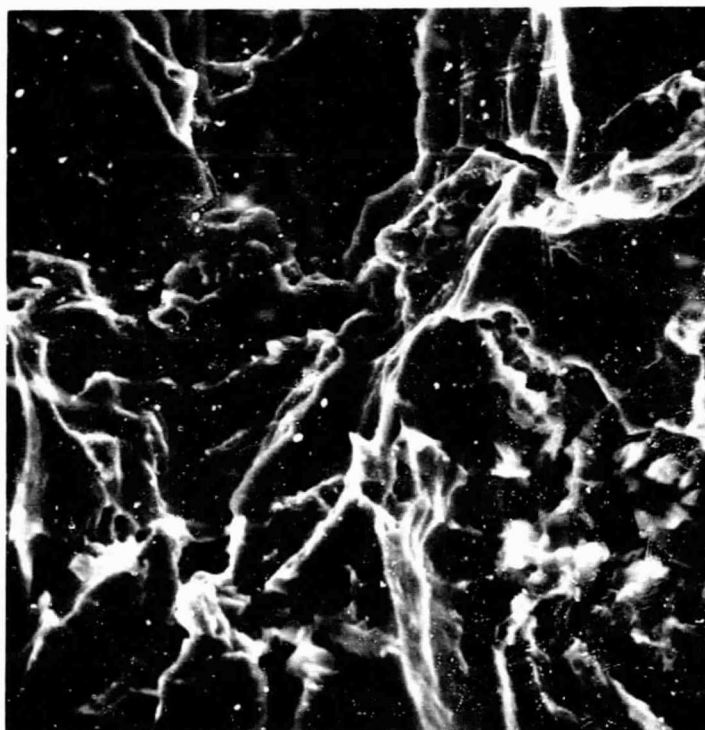
493X

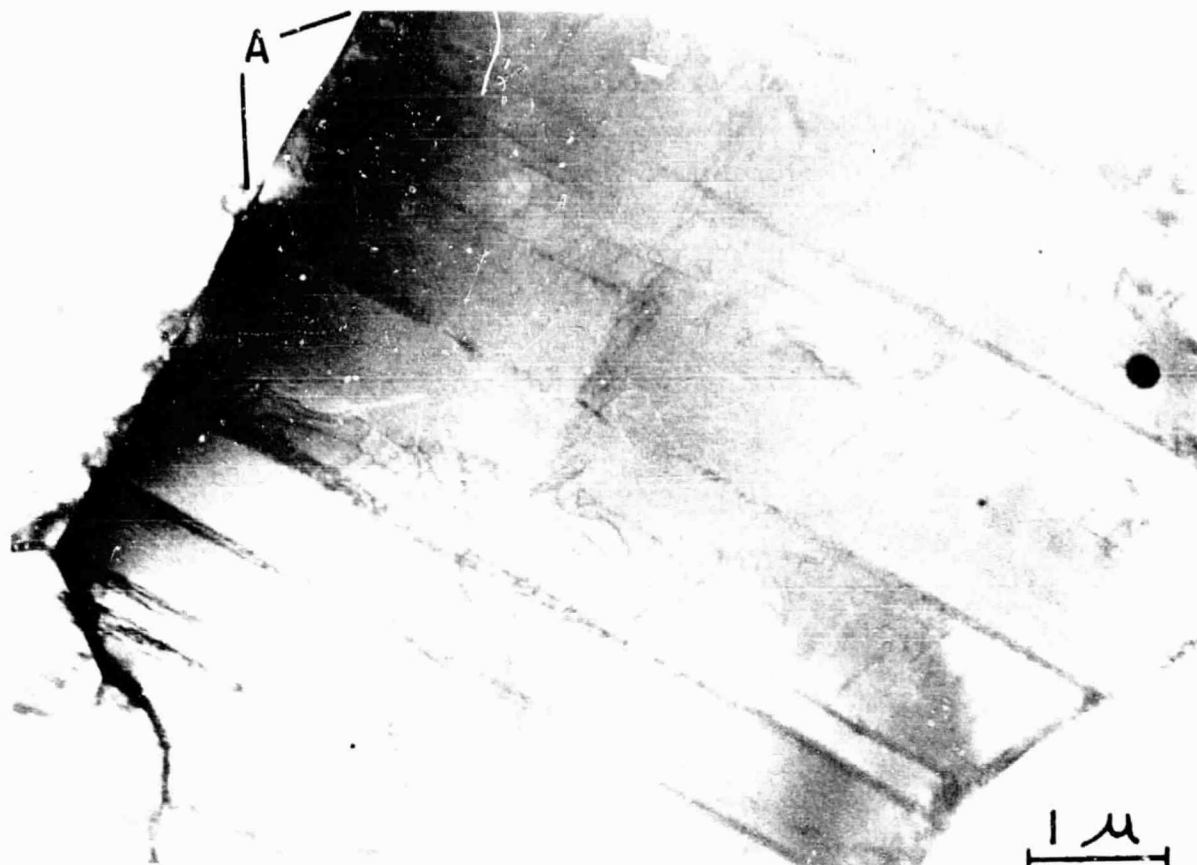FIGURE 3. SCANNING ELECTRON MICROGRAPH OF
Ti-4Al FRACTURED IN AIR
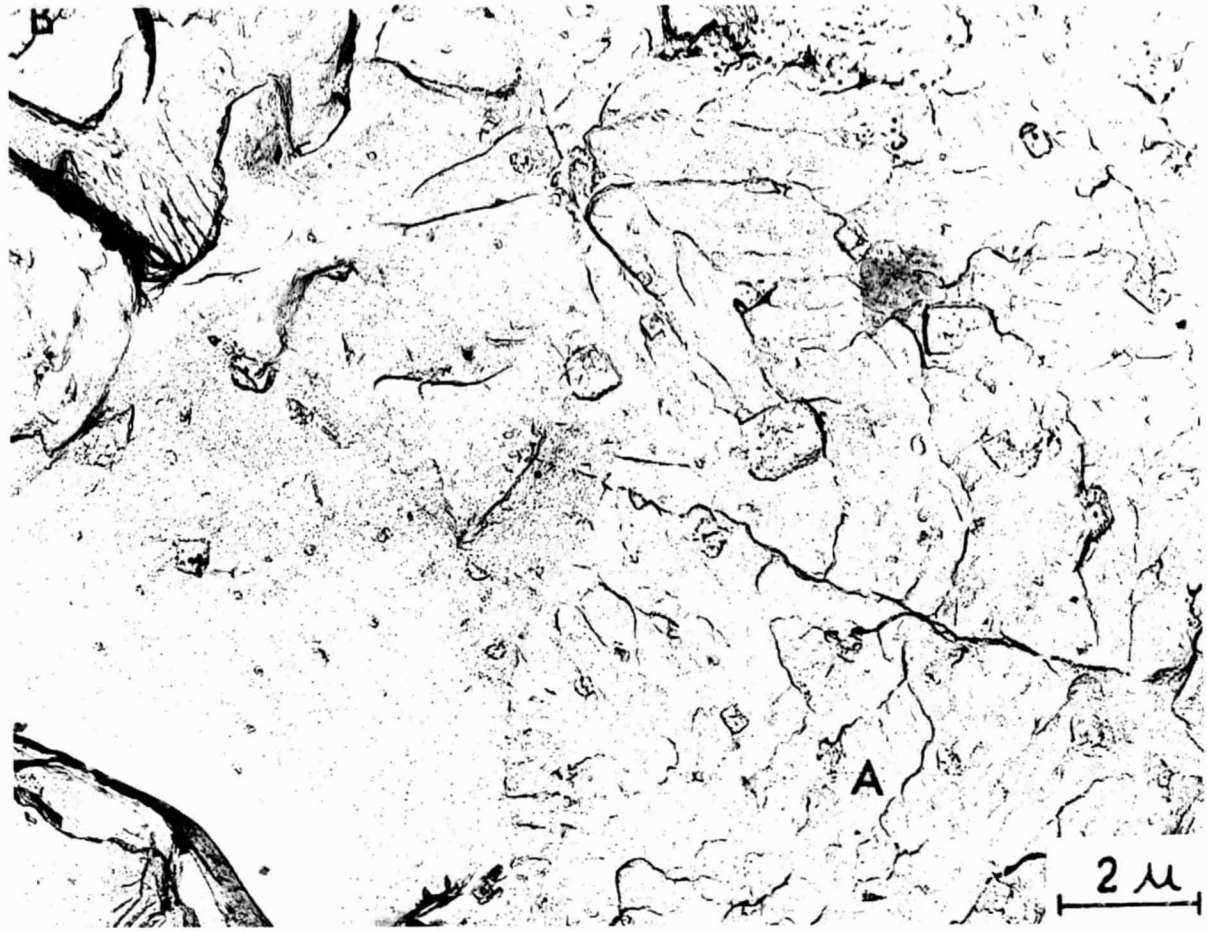
a.

b.

FIGURE 4.   ELECTRON-REPLICA MICROGRAPHS OF A SALT-WATER STRESS-
CORROSION FRACTURE IN Ti-8Al-1Mo-1V

BATTELLE MEMORIAL INSTITUTE – COLUMBUS LABORATORIES

a. Shows Coplanar Slip on (10$\bar{1}$0) and Some Nonprism Slip
Note large steps where (10$\bar{1}$0) slip planes interest a
grain boundary, e.g., at A.

2V171

b. Shows Intragranular β Particles Sheared by Slip on (10$\bar{1}$0)

FIGURE 5. Ti-8Al-1Mo-1V, 70 PPM HYDROGEN, ϵ = 2.5 PERCENT

The transition from irregular tangles of dislocations to coplanar arrays is probably related to the presence of ordered Ti$_3$Al precipitates in alloys containing greater than 7 weight percent aluminum. It has not been possible to image the ordered particles in dark field, but superlattice reflections are seen in the diffraction patterns from annealed specimens (Figure 6). The passage of an a<11$\bar{2}$0> dislocation through an ordered precipitate creates an antiphase boundary, and a second a<11$\bar{2}$0> dislocation is required to restore the correct nearest-neighbor relations across the slip plane. Consequently, the dislocations glide as pairs separated by a ribbon of antiphase boundary and are confined to their primary slip planes. Furthermore, the passage of successive dislocations decreases the area of ordered region per unit area of slip plane, and the stress to move subsequent dislocations over the same plane will be less.

Crack-Velocity Measurements

A procedure has been established for measuring the rate of crack propagation during notched-cantilever stress-corrosion tests. Figure 7 shows the crack-velocity measurements for Ti-8Al-1.5Mo-0.5V plotted as a function of crack length. The fatigue crack was abnormally long in this specimen so the crack length at the beginning of stable crack growth was 0.76 centimeters. The crack velocity increased continuously from the onset of slow crack growth until the test was stopped just before the rapid final fracture. However, the crack acceleration decreased sharply and the velocity reached a limiting value of 6.8×10^{-3} centimeter per second. Since the stress intensity at the tip of the crack increases with crack length, the crack velocity would be expected to increase continuously during stable crack growth, provided the crack velocity is limited by the mechanics of fracture. Apparently, the rate of slow crack growth during aqueous stress-corrosion cracking of titanium alloys is limited by the flux of some active species to the crack-tip region. An effort is being made to identify this active species by determining the temperature and stress-intensity dependences of the limiting crack velocity.

Hydrogen Effects

There is considerable evidence that the susceptibility of titanium alloys to aqueous stress-corrosion cracking is related to the hydrogen which is produced by the cathodic reaction,

$$H^+ + e^- \rightarrow H .$$
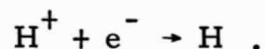
Accordingly, a thorough study was made of the rate of absorption of hydrogen by titanium alloys, the solubility of hydrogen and the nucleation of hydrides, and the effect of dissolved hydrogen on the mechanical properties.

The rate of hydrogen absorption was measured by observing the pressure in the reaction system of a Sieverts apparatus as a function of time while charging specimens with hydrogen at 650 C. To date three alloys have been studied: Ti-4Al-3Mo-1V annealed, Ti-13Al annealed 70 hours at 920 C and step cooled, and Ti-13Al annealed 18 hours at 1050 C and quenched. Ti-13Al is an all-α alloy. The 920 C anneal produces a high volume fraction of the ordered Ti$_3$Al phase, and the 1050 C anneal results in a single-phase α solid solution. The amount of hydrogen absorbed by each alloy as a function of time at 650 C is shown in Figure 8*. As expected, the rate of hydrogen absorption by

* In Figure 8 the curves for the titanium-13 weight percent aluminum specimens are labeled as atomic percent (titanium-20 atomic percent aluminum).
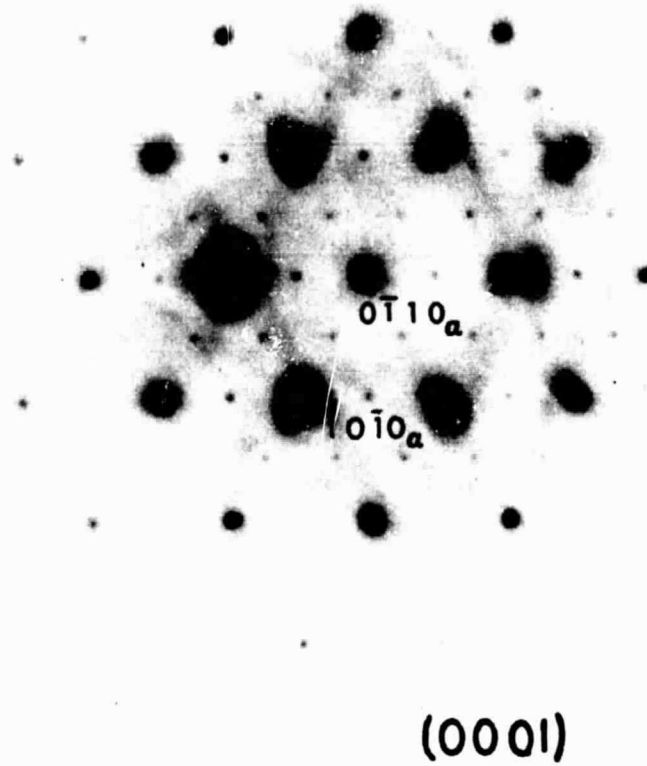
23

(0001)

FIGURE 6. DIFFRACTION PATTERN FROM ANNEALED Ti-8Al-1Mo-1V

Note: Superlattice reflections at positions $(h/2, \ k/2 \cdot \ell)_\alpha$.
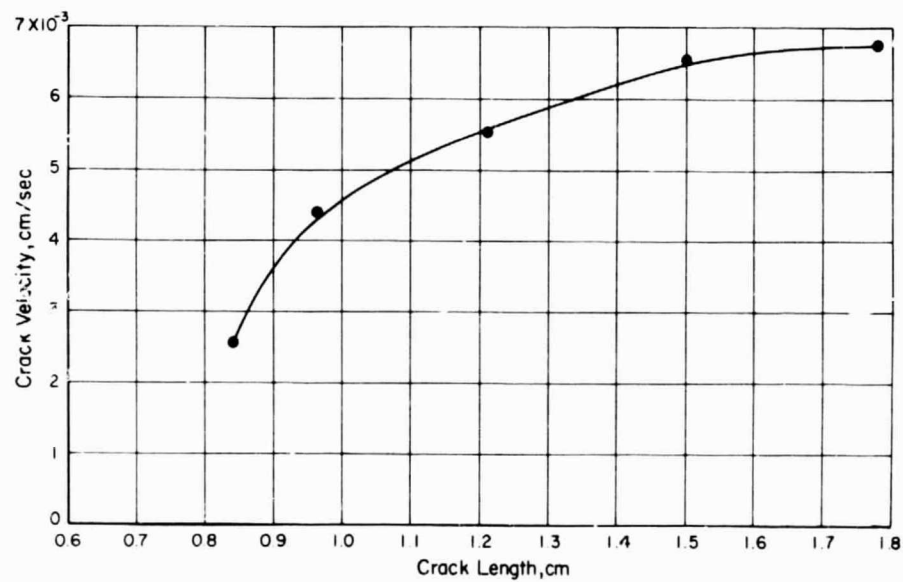

FIGURE 7. VELOCITY OF STRESS-CORROSION CRACK
FOR Ti-8Al-1.5Mo-0.5V IN SALT WATER

Ti-4Al-3Mo-1V is relatively rapid owing to the high solubility of hydrogen in the β phase. The interesting result is that the alloy containing ordered Ti_3Al absorbs hydrogen at about twice the rate for an identical disordered alloy. This result explains the observations of other workers that the volume of hydride resulting from hydrogen pickup during chemical polishing increases with the aluminum content of the alloy. It has been argued that increasing the aluminum content makes hydride nucleation easier. However, Battelle's studies of hydride nucleation (reported later) suggest that the opposite is true, and that the increase in the volume of hydride with aluminum content is due to the enhanced rate of hydrogen absorption by Ti_3Al.

Hydrogen solubility and hydride nucleation were studied by charging specimens in a Sieverts apparatus at 650 C to various total hydrogen contents and examining the as-charged specimens by transmission electron microscopy. It was found that up to 800 ppm of hydrogen can be added to Ti-8Al-1Mo-1V before hydrides form. The hydrides appear to nucleate randomly and grow rapidly on $\{10\bar{1}0\}$ until they impinge (Figure 9). The volume fraction of hydride was estimated by linear analysis, and the partition of hydrogen between hydride and the α matrix was calculated. In this way it was shown that all of the available hydrogen is in the form of hydride, and that the equilibrium solubility of hydrogen in α containing 8 weight percent aluminum is negligible. In other words, the addition of aluminum to α titanium makes hydride nucleation more difficult, but does not appreciably change the equilibrium solubility of hydrogen.

If there is a nucleation barrier for the formation of hydrides in Ti-Al alloys, then an activation energy must be somehow provided before hydrides will nucleate from supersaturated solid solution. In the experiment first described the activation energy was provided by a large hydrogen supersaturation. It can also be provided by small amounts of plastic strain. When specimens containing at least 200 ppm of hydrogen are deformed to about 2 percent plastic strain, hydrides nucleate on the active $\{10\bar{1}0\}$ slip planes and grow rapidly to consume all of the available hydrogen (Figure 10). The strain-induced hydrides formed during deformation at all strain rates that were investigated ($\dot{\epsilon} = 3 \times 10^{-3} - \dot{\epsilon} = 3/minute$).

The effect of dissolved hydrogen on the mechanical properties was investigated by deforming a series of 0.020 inch-thick tensile specimens of Ti-8Al-1Mo-1V at various strain rates and hydrogen contents. The stress-elongation curves are shown in Figure 11, and the tensile data are summarized in Table 9. The yield stress and initial rate of work hardening increase with hydrogen content and strain rate, but the ductility shows little dependence on these parameters except in the 400 ppm specimen at the

TABLE 9. EFFECT OF HYDROGEN CONTENT AND STRAIN RATE ON THE TENSILE PROPERTIES OF Ti-8Al-1Mo-1V

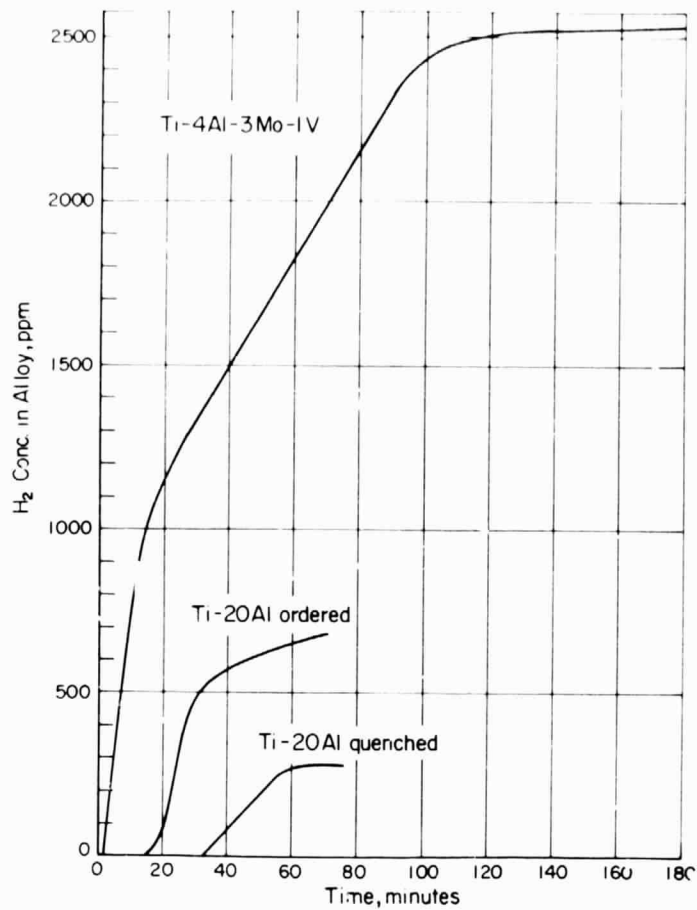| Specimen	Hydrogen Content, ppm	$\dot{\epsilon}$/min	0.2% Offset Yield Strength, ksi	Ductility, percent	
				Reduction in Area	Elongation
D	80	3×10^{-3}	126.5	22	16.9
C	80	3	141.8	18	13.8
B	400	3×10^{-3}	145.0	24	19.8
A	400	3	154.8	7.1	1.1

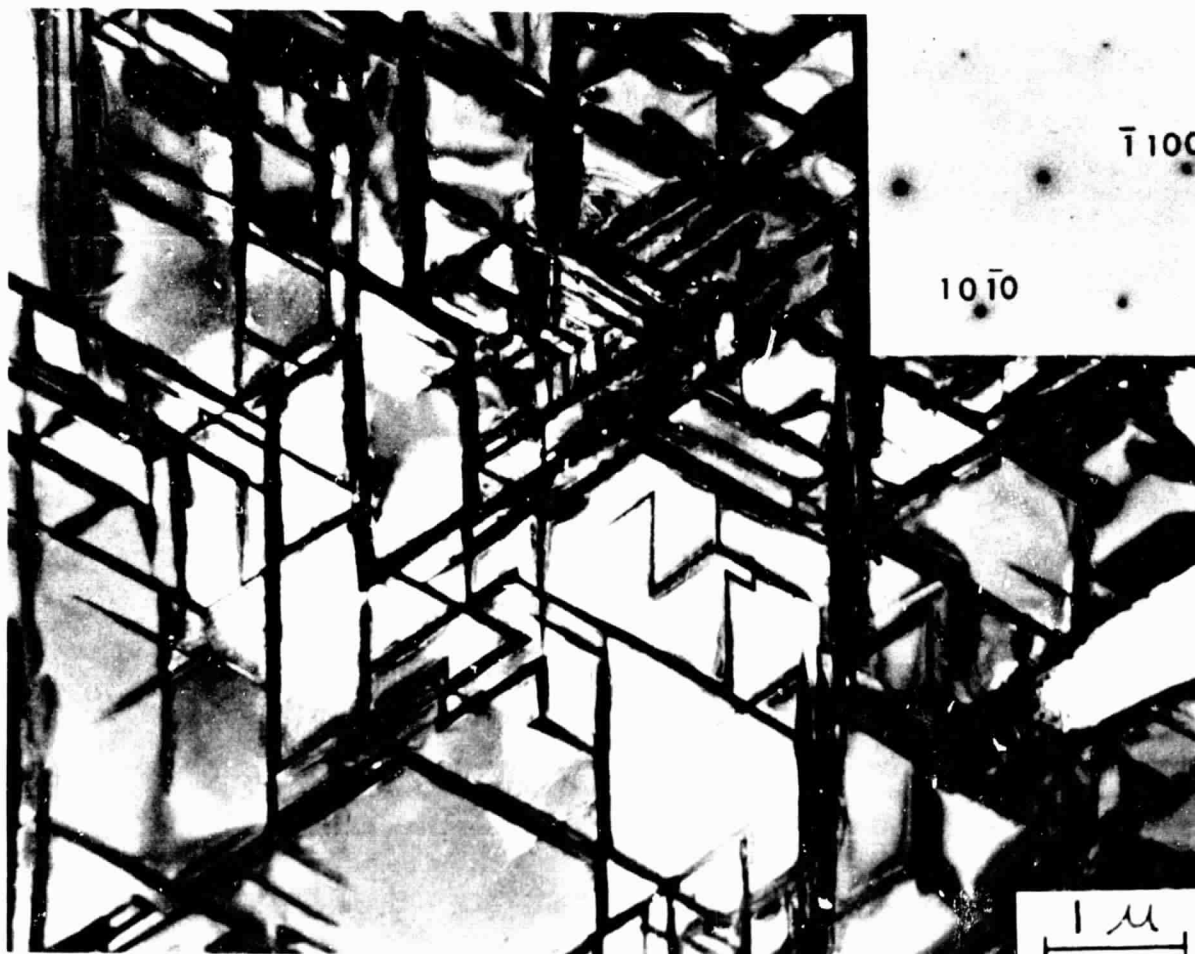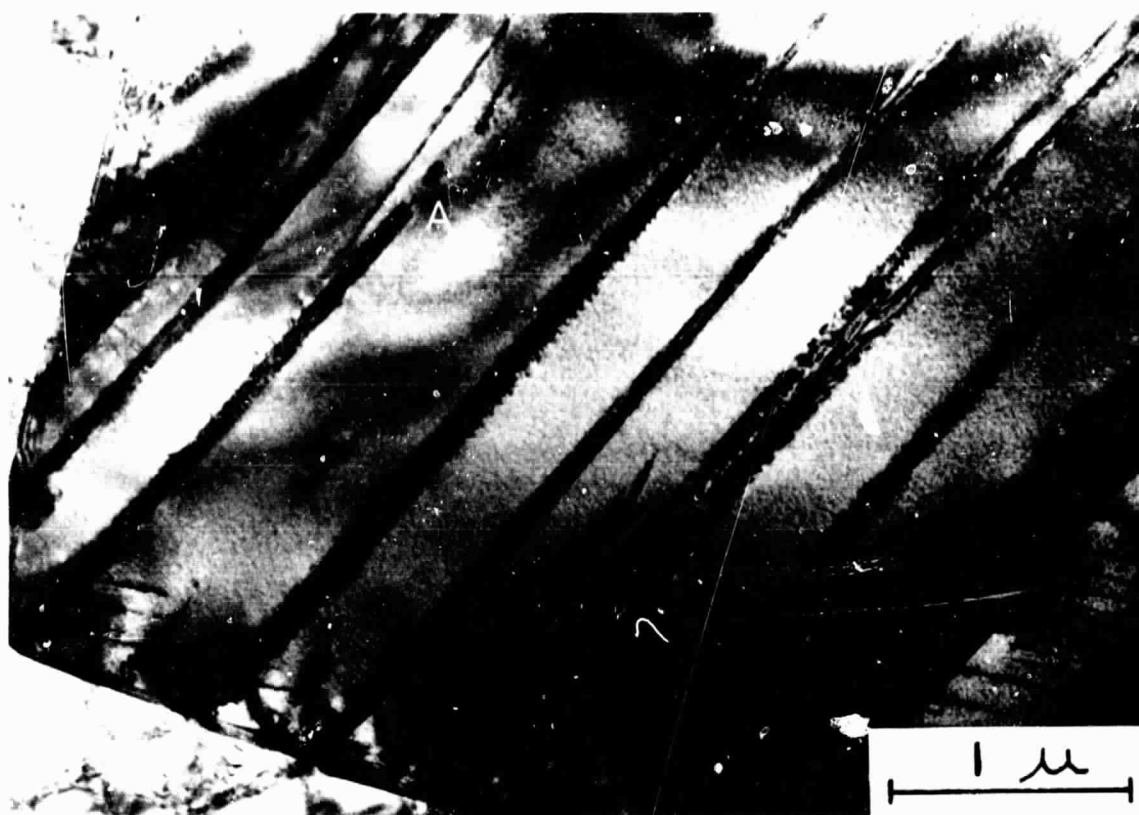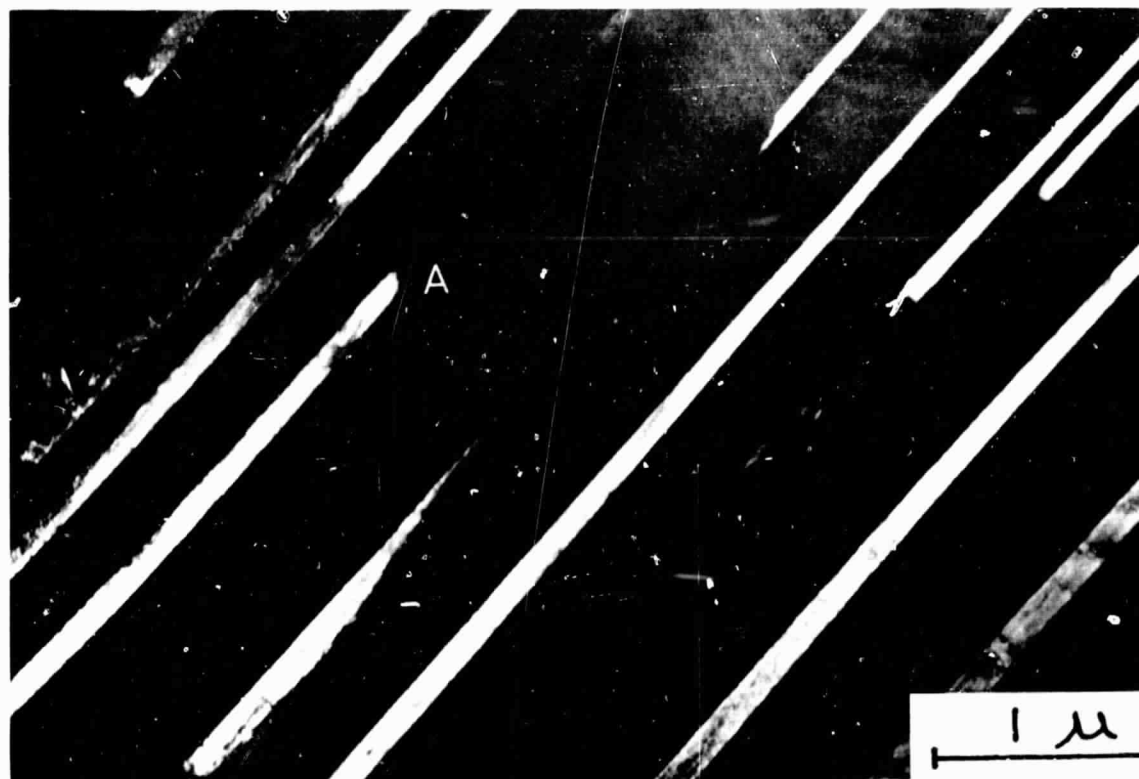FIGURE 8.   RATES OF HYDROGEN ABSORPTION AT 650 C

FIGURE 9.   SPECIMEN CHARGED WITH 800 PPM HYDROGEN, SHOWING
SPONTANEOUSLY NUCLEATED HYDRIDES

a. Strain-Induced Hydrides Lying in (10$\bar{1}$0) Slip Planes

b. Same Area as Above; Dark-Field Micrograph From Hydride Reflection

FIGURE 10. Ti-8Al-1Mo-1V, CHARGED TO 400 ppm HYDROGEN AND
DEFORMED 3 PERCENT

higher strain rate*. Thus, it is clear that hydrogen entering this alloy in the vicinity of a stress-corrosion crack will "harden" that region for all strain rates in the range expected for stress-corrosion cracking. Furthermore, it is possible that mechanical embrittlement occurs when the strain rate is in excess of 3/minute.
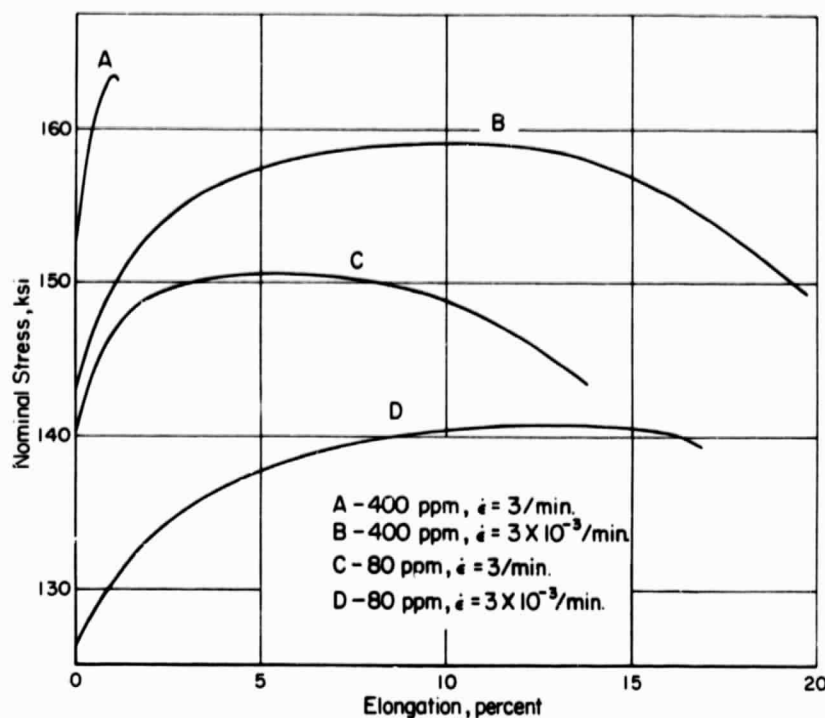
FIGURE 11. ROOM-TEMPERATURE TENSILE PROPERTIES
OF Ti-8Al-1Mo-1V

Mechanism of Aqueous Stress-Corrosion Cracking

The important observations on the aqueous stress-corrosion of titanium alloys are:

(1) Susceptibility depends critically on the aluminum content. The marginal composition is approximately 7 weight percent aluminum. Alloys containing greater than 7 weight percent aluminum are susceptible regardless of heat treatment or amount or kind of β-stabilizing elements.

(2) With increasing aluminum content in the α phase, cross slip becomes more difficult and slip is confined to coarse slip bands. The coplanar dislocations form long pileups which produce stress concentrations at grain boundaries and α/β interfaces.

(3) Hydrogen is absorbed more rapidly by an alloy containing Ti_3Al than by a disordered alloy.

(4) With increasing aluminum content the nucleation of hydrides in the α phase becomes more difficult, but strain-induced hydrides can nucleate in the active $\{10\overline{1}0\}$ slip planes when the total hydrogen content is as low low as 200 ppm.

---

*The low ductility shown by Specimen A may be inaccurate because fracture initiated at the shoulder of the gauge length. This test is being repeated using a different specimen geometry.

(5) The aqueous stress-corrosion fracture results from cleavage-like fracture of certain α grains and subsequent ductile failure of the remaining material.

(6) The velocity at which a stress-corrosion crack propagates reaches a constant value, which is independent of the stress intensity at the root of the crack.

(7) The inherent fracture toughness is not affected by exposure to an aqueous environment.

(8) The yield stress and initial rate of work hardening in alloys containing hydrogen increase with hydrogen content and strain rate.

To this list should be added the following facts that have been established by other workers:

(9) The cleavage plane in Ti-Al alloys is close to (0001).[1]

(10) After being exposed to salt water for long times at a subcritical stress, or after being charged with hydrogen by chemical polishing, susceptible alloys often contain hydrides, whereas immune alloys do not.[2]

Titanium alloys fail at low stress intensities in aqueous environments because cleavage microcracks are nucleated in the vicinity of the main crack (Figures 2 and 4). The cracking mechanism is the sequence that leads to the nucleation of cleavage cracks in material that would otherwise fracture in a ductile manner.

The experiments of Scully and his co-workers[3] establish a very good correlation between the appearance of hydrides in an alloy and its susceptibility to stress-corrosion cracking. Therefore, hydrogen must play an important role in the formation of the cleavage cracks. Battelle experiments have shown that the rate of hydrogen absorption increases markedly with the amount of ordered Ti_3Al in the α phase (Figure 8), and it is suggested that it is the ease with which an alloy can absorb hydrogen, not the ease of hydride nucleation, that contributes to its susceptibility. This interpretation is consistent with all observations by Scully, et al., and with Battelle's conclusion that increasing the aluminum content of the α phase makes hydride nucleation more difficult. The correlation between aluminum content (volume fraction of Ti_3Al) and susceptibility to stress-corrosion cracking has been recognized for several years. It is usually attributed solely to the fact that ordered precipitates inhibit cross slip in α grains and result in coplanar dislocations (Figure 5). This is generally a more susceptible microstructure than the tangled cell structure that occurs when cross slip is easy. Now it must be considered that the aluminum content also affects the ease with which a titanium alloy can absorb hydrogen.

The next question is: How does absorbed hydrogen contribute to cleavage-crack formation. There are three possibilities:

(1) The amount of plastic flow around the crack tip is reduced, and this increases the stress concentration at the crack tip (i.e., the cracks are "sharper" in an aqueous environment).

(2) The cleavage strength of the alloy is reduced by hydrogen adsorption.

(3) Hydrogen absorption leads to accelerated electrochemical attack on the cleavage plane or precipitation of a brittle compound on the cleavage plane.

The results of tensile tests (Figure 11) show that dissolved hydrogen raises the yield stress of Ti-8Al-1Mo-1V significantly. This suggests that hydrogen absorption does restrict the amount of plastic relaxation around a crack. Further experiments are planned to measure directly the size of the plastic zones around cracks in specimens loaded to the same stress intensity in air and in salt water. Hydrogen can affect yielding in titanium alloys in two ways:

(1) By raising the lattice friction stress due to interaction between dislocations and dissolved hydrogen.

(2) By precipitating as hydride and blocking dislocation movement.

In order to choose between these possibilities, some estimate must be made of the amount of hydrogen that is likely to be absorbed by a titanium alloy during aqueous stress corrosion. Beck[4] has devised an electrochemical model which shows that, because of the low rate of hydrogen discharge by the cathodic reaction and the high crack velocity, the hydrogen concentration in the alloy is virtually unchanged. Following his procedure, for a crack velocity of 5×10^{-3} cm/sec, the concentration of hydrogen at the fracture surface is estimated to be 20 ppm at a distance of 100 A from the crack tip and 200 ppm at 1 micron from the crack tip. This represents the hydrogen that is released by the cathodic reaction and which then diffuses into the alloy. Since Ti-8Al-1Mo-1V has a base hydrogen content of about 80 ppm, the total concentration during stress corrosion could be as much as 100 ppm at 100 A from the crack tip and 280 ppm at 1 micron from the crack tip. In this model, the hydrogen concentration is maximum at the fracture surface and decreases rapidly going into the alloy. Clearly, the effects of absorbed hydrogen must be confined to the thin layer of material adjacent to the crack surface. Consequently there cannot be any dislocation-hydrogen interaction or hydride precipitation throughout the grains surrounding the crack.

However, the calculations indicate that the hydrogen concentration in the thin layer adjacent to the crack surface is sufficiently high for strain-induced hydrides to form in the slip planes. Therefore, it is suggested that where active $\{10\bar{1}0\}$ slip bands emerge at the crack surface, at distances greater than 1 micron behind the crack tip, hydrides nucleate in the slip planes and prevent the emergence of glide dislocations. Since cross slip is difficult, a pileup ensues, and further dislocation movement ceases when the back stress equals the resolved shear stress. In this way the plastic zone is confined to within one or two grain diameters of the fracture face, and the stress concentration at the crack tip is much higher than what it would be in air at the same applied stress. The tensile stress produced by the dislocation pileups will be a maximum across a plane normal to the $\{10\bar{1}0\}$ slip planes and this is consistent with the observed (0001) cleavage plane. Note that any mechanism based on accelerated dissolution of hydrides in the slip planes, or stress-fracture of the hydrides in the slip planes can be discounted because the observed cleavage plane would then be $\{10\bar{1}0\}$. Efforts to substantiate this mechanism by direct observation of hydrides in specimens that have been fractured in salt water have so far been unsuccessful. A new technique is presently being employed for cutting electron-microscope specimens from the vicinity of the crack tip. Hopefully, it

will be possible by transmission electron microscopy to examine areas that are near enough to the crack tip to show the dislocation microstructure and the origin of the cleavage cracks

It is entirely possible that the blocking of slip planes by hydrides is not the only, or even the principal, cause of the cleavage cracks that lead to stress-corrosion failure. All of the above arguments show how the maximum tensile stress at the crack tip can be increased in an aqueous environment. At the same time, the stress required to nucleate a cleavage crack could be reduced by the adsorption of some surface-active species at the crack tip. The crack velocity measurements which are now in progress will provide kinetic data that will determine the rate-controlling process. In this way the critical species in the environment can be identified.

N_2O_4 Environments

Thermodynamic Considerations

The following facts are pertinent to the study of the mechanism of stress-corrosion cracking in N_2O_4.

(1) Stress-corrosion cracking occurs when no significant amount of NO is present (red N_2O_4) and the system is exposed to moderately high stresses in the temperature range 85 to 165 F.

(2) In the presence of excess NO, stress-corrosion cracking of titanium does not occur (green N_2O_4).

(3) Chloride-ion addition as NOCl to green N_2O_4 does not initiate cracking.

(4) Stress-corrosion cracking occurs in green N_2O_4 which has been oxygenated.

(5) Addition of H_2O to red N_2O_4 eliminates stress-corrosion cracking.

Thermodynamic data for reactions of water with N_2O_4 have also been reported. Consideration of these thermodynamic data (Table 10) indicates that water does react

TABLE 10. THERMODYNAMIC DATA FOR POSTULATED REACTIONS IN N_2O_4

Reaction	ΔG° Standard Free Energy of Reaction, kcal at 298 K (77 F)
(1) $N_2O_4(\ell) + \frac{1}{2} O_2(g) + H_2O(\ell) \rightleftharpoons 2HNO_3(\ell)$	-4.622
(2) $\frac{3}{2} N_2O_4(\ell) + H_2O(\ell) \rightleftharpoons 2HNO_3(\ell) + NO(g)$	+4.434

spontaneously with N_2O_4 in the presence of oxygen, but on the other hand, water does not react spontaneously with N_2O_4 to produce nitric acid if NO is present. The analytical data reported for red and green N_2O_4 are given in Table 11.

TABLE 11. COMPOSITION OF RED AND GREEN N_2O_4-PLANT ANALYSIS[a]

Analysis	Red N_2O_4, MIL-P-26539B	Green, MSC-PPD-2A
N_2O_4, percent	99.99	99.26
NO, percent (Colorimetric)	--	0.81; 0.86[b]
NO, percent by MSC-PPD-2A	--	0.72
H_2O, percent	0.05	0.05
Cl as NOCl, percent	0.001	0.001
CO_2, percent	0.028[c]	0.045[c]
Oxygen, percent	0.006[d]	0.002[d]
Particulate, mg/liter	2.3	3.1

(a) Hercules Incorporated, Hercules, California.

(b) Obtained on last 10 grams of retained sample.

(c) Results are bare because of inclusion of gas freezing. Actual percentage of CO_2 could be two times the reported value.

(d) Argon is included in this test. The data in Table 2 clearly indicate that green N_2O_4 has a significant amount of nitric oxide compared with the red N_2O_4. It is significant that the reported H_2O contents do not distinguish the protonated species.

It is apparent from Table 10 that red N_2O_4 will contain nitric acid according to Reaction (1), and a certain HNO_3/H_2O ratio exists when the solution is at equilibrium. In green N_2O_4, Reaction (2) occurs in the reverse direction (i.e., right to left as written in Table 10, and this solution also contains a certain equilibrium HNO_3/H_2O ratio. It is postulated that a certain critical HNO_3/H_2O ratio is required to produce stress-corrosion cracking of titanium alloys in N_2O_4. The marked difference in behavior of red N_2O_4 and green N_2O_4 indicates that the HNO_3/H_2O ratio in red N_2O_4 is above the critical value for stress corrosion cracking, while the HNO_3/H_2O ratio in green N_2O_4 is less than the critical value. Following the procedure outlined in earlier reports, the ratio $[HNO_3]/[H_2O]$ is calculated to be 6016 for red N_2O_4 and 5 for green N_2O_4.

Similar calculations show that additions of water to red N_2O_4 reduces the $[HNO_3]/[H_2O]$ ratio to a value of the order of 1. It should be noted that the literature reports no stress-corrosion cracking of titanium in red N_2O_4 to which either 0.6 percent H_2O of 0.10 percent NO is added.[1] It is readily seen from the above calculations that additions as small as 0.24 percent H_2O or 0.22 percent NO would be expected to inhibit the stress-corrosion cracking of titanium in red N_2O_4, depending upon the HNO_3/H_2O ratio. This work suggests that it is not the inhibitive character of NO or H_2O entities which is the most important factor but rather the HNO_3/H_2O ratio that is produced by the presence of these entities. Although the addition of water to red N_2O_4 would be expected to produce HNO_3 according to Reaction (1) the extent of the reaction is determined by the initial oxygen concentration. Consequently, upon the addition of, e.g., 0.6 percent H_2O, only a very small amount reacts to produce HNO_3 while the remainder is unreacted. The HNO_3/H_2O ratio is thus decreased from its initial value.

Although the addition of water to red N_2O_4 decreases the HNO_3/H_2O ratio in the presence of small amounts of oxygen (6 x 10^{-3} percent), this will not be true in the presence of excess oxygen. In the presence of excess oxygen, i.e., as in the preparation of red N_2O_4 from green N_2O_4, the HNO_3/H_2O ratio will be increased by the addition of water since Reaction (1) proceeds completely "to the right". An experiment has been conducted with U-bend specimens of Ti-6Al-4V alloy in both the solution-treated-and-aged (STA) and annealed conditions. The specimens were exposed to green N_2O_4 at 105 F, doped with 0.028 g $H_2O/100$ g N_2O_4, and pressurized to 250 psi with oxygen. As noted above, it was believed that the addition of water to either green or red N_2O_4 would be converted to HNO_3 in the presence of excess oxygen and produce a HNO_3/H_2O ratio likely to induce stress-corrosion cracking in titanium. The magnitude of the water addition was chosen such that the value would not be too unrealistic of the value (7.8 x 10^{-4} moles $H_2O/100$ g N_2O_4 by theoretical calculation) present in the starting material. The water addition, however, was required to be a reasonable value such that in later experiments, accurate samples of tritiated water could be used. An addition of 0.028 g $H_2O/100$ g N_2O_4 (i.e., 0.20 ml H_2O per 500 ml N_2O_4) met these requirements. After 7 days the specimens were removed and failures noted for both the STA and annealed alloys. The failures had occurred at the apex of the U-bend, and, while there were numerous microcracks on the outer side, there appeared to be only one crack line on the inner side of the U-bend. The specimens were untarnished on the outer metal surface but the fracture surface was observed to be dark golden on the outer edge and dull-gray on the inner edge.

Cl^{36} Tracer Study of Titanium Corrosion by N_2O_4

The role of chloride ions in stress-corrosion has been documented for a number of metals and alloys, including titanium. For example, Rideout[5] found chloride concentrations of 0.1 to 2 $\mu g/cm^2$ on the surface of titanium after contact with NaCl solutions. In order to determine whether chloride absorption is involved in the stress-corrosion cracking of titanium alloys in N_2O_4, some specimens were exposed to N_2O_4 containing Cl^{36} isotopes. Three specimens of titanium were exposed to red N_2O_4 containing 100 ppm Cl^{36} for 4 hours at 105 F. Following exposure the activity of each specimen was determined using a proportional counter, and the amount of chloride absorbed by each was calculated (Table 12).

Only small differences in chloride absorption were found between stressed and unstressed specimens, and it is concluded that chloride ions are not preferentially observed at the crack initiation sites. Approximately 5 x 10^7 β/cm^2 are needed for an autoradiograph, and 2 to 3 months' exposure would be required for the uniformly stressed pieces, the most radioactive specimens. Since it appeared unlikely that really useful information would be gained from these, no autoradiographs were made.

Electron Microscopy of Exposed Thin Foils

Specimens of Ti-6Al-4V representing the STA condition and the annealed condition were prepared in the form of 0.005-inch-thick strips. These were electrolytically thinned at the region of maximum strain until perforations occurred, and exposed under stress to red and green N_2O_4 at 105 F.

TABLE 12. ABSORPTION OF CHLORIDE FROM N_2O_4 BY TITANIUM

Description of Specimen	Thickness, mils	Area Counted, cm^2	Activity D/M[a]	Activity D/M/Cm^2	Total Cl, $\mu g/cm^2$
		Unstressed Specimens			
Square, slightly curved	~5	1.9	45	23.5	0.0065
Square, round corner	~5	5.5	105	19.5	0.0055
Long narrow piece	~5	2.2	40	17.0	0.005
		Stressed Specimens			
Bowed specimen, scratch	~50	~2[b]	40	20	0.0055
Bowed specimen, no scratch	~50	~2[b]	70	35	0.010
Uniformly stressed, No. 5 (broken)	~5	2.3	0	--	--
Uniformly stressed, No. 1	~5	2.3	280	120	0.032
Uniformly stressed, No. 3	~5	2.3	260	110	0.032
Uniformly stressed, No. 4	~5	2.3	190	85	0.025
Stainless steel specimen holder (No. 5)	~7[c]	--	6500	930	0.32

(a) Based on an efficiency for Cl^{36} of 16 percent on second shelf of RIDL counter.
(b) Estimated approximate area viewed by counter.
(c) Geometric area of upper face of holder; etched, matte finish.

FIGURE 12. Ti-6Al-4V, STA, STRESSED IN RED N_2O_4, SHOWING CRACK
RUNNING PARALLEL TO MARTENSITE INTERFACES

BATTELLE MEMORIAL INSTITUTE – COLUMBUS LABORATORIES

Unfortunately, the conditions were not satisfactory for observing the sites of crack initiation in any of the specimens. The specimens in the STA condition exposed to red N_2O_4 or green N_2O_4 fractured completely across the section of maximum stress and exhibited many cracks propagating in from the edges of the thinned regions. There was no evidence of cracks initiating on the flat surface of the specimen. None of the other specimens showed any evidence of cracking or corrosive attack. The microstructure of Ti-6Al-4V in the STA condition consists of roughly equal proportions of equiaxed α grains and equiaxed regions containing transformed α and β. The transformed regions consist of β particles precipitated in a matrix of α'' martensite plates. The fracture path in the STA specimens was almost entirely confined to the $\alpha'' + \beta$ areas and often ran parallel to martensite interfaces. An example of this behavior is shown in Figure 12. There was little evidence of plastic deformation around cracks in the $\alpha'' + \beta$ region, but much deformation and buckling of the foil was observed around cracks in α grains. Often, secondary cracks were arrested in an α grain by the massive plastic deformation at the crack tip.

Fractography

Specimens of Ti-6Al-4V in the STA condition were cracked in N_2O_4 pressurized to 250 psi with an oxygen atmosphere. Optical examination of the fractures showed that the initiating edge had a light-brown tarnish film. The remainder of the fracture surface had a dull metallic appearance. Figures 13a and 13b are scanning-electron micrographs showing the transition region between the brown tarnished area and the dull-metallic area. The metallic area at the bottom is characteristic of ductile rupture. The tarnished area at the top appears to be primarily a transgranular brittle fracture covered with a corrosion-product film. The evidence of corrosion products is more pronounced at the initiating edge of a fracture in Figure 14. Note the bright spots that indicate electron charging of nonconducting materials. Also, although the fracture path appears to have followed crystallographic planes within grains, the edges are not sharp as one might expect from a completely mechanical fracture. This rounding of edges may be the result of the formation of an oxide on the surface, or the corroding away of edge material, or both. At this time it is not known if the microcracks on the fracture face are in the metal or in a relatively thick oxide film.

Methanol Environments

Exposure Tests

The experimental alloys were exposed to dry methanol at 90 percent of their 0.2 percent offset yield strength. These stresses were obtained by constant deflection of sheet specimens in stainless steel three-point-loading fixtures. The specimens were insulated from the fixtures with thin plastic spacers. The results of these exposures are given in Table 13. All of the specimens of the alloys containing 8 weight percent aluminum cracked into two separate pieces, whereas most of the specimens of 4Al-base alloys appeared to have many small cracks at the end of the test.
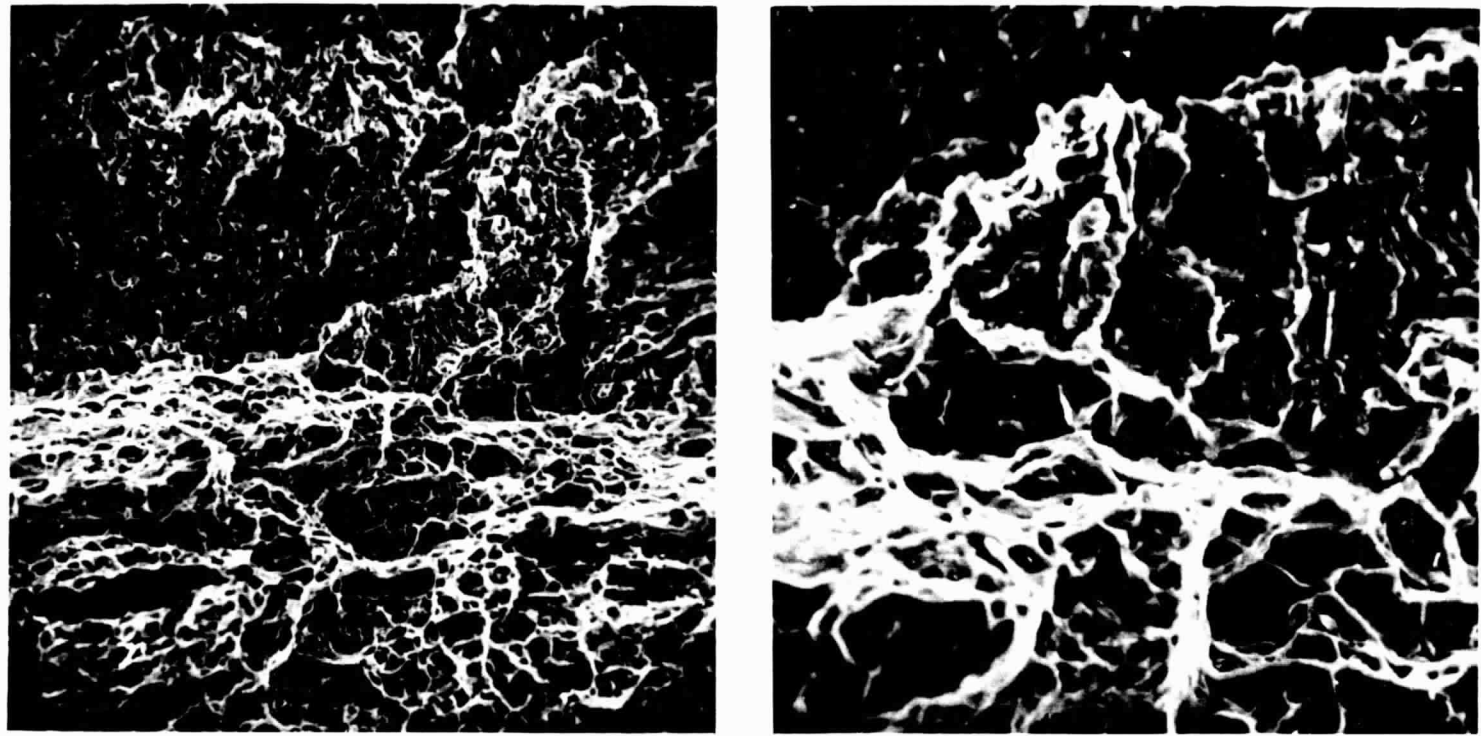
500X   SE172   2000X   SE168

FIGURE 13.   SCANNING-ELECTRON MICROGRAPHS OF N_2O_4 STRESS-CORROSION
FRACTURE IN "ANNEALED" Ti-6Al-4V, SHOWING BRITTLE AND
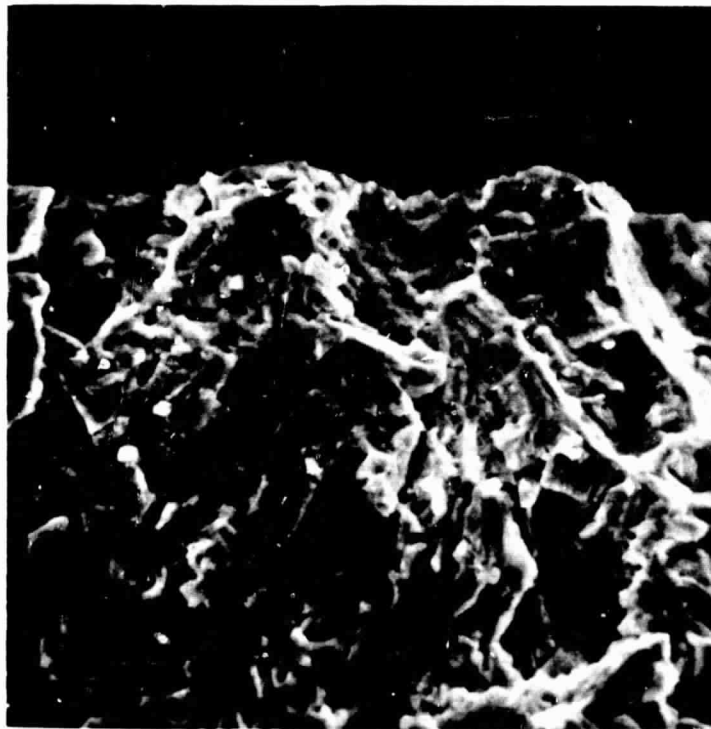DUCTILE REGIONS

FIGURE 14.   SCANNING-ELECTRON MICROGRAPHS OF N_2O_4 STRESS-CORROSION
FRACTURE IN Ti-6Al-4V, SHOWING THE INITIATING EDGE

TABLE 13. STRESS-CORROSION CRACKING OF TITANIUM IN METHANOL

Alloy Nominal Composition, percent	Code	Stress Level, ksi	Time to Failure and Remarks
Ti-4Al-1.5Mo-0.5V	2	92	Did not fail completely; small cracks noted after 172 hours at 7X
Ti-8Al-1.5Mo-0.5V	77	117	7 to 21 hours
Ti-4Al-3Mo-1V	0	103	Did not fail completely; small cracks noted at end of test - 15 days
Ti-8Al-3Mo-1V	4	127	3-1/2 hours
Ti-4Al-3Mo	8	99	Did not fail completely; small cracks noted at end of test - 15 days
Ti-4Al	67	60	Did not fail completely; small cracks noted at end of test - 27 days
Ti-8Al (commercial)	3	90	55 to 70 hours
Ti-4Al-3Mo-1V (commercial)	41	110	151 hours
Ti-8Al-1Mo-1V	81	111	7 to 21 hours
Ti-4Al-4V	9	95	151 hours
Ti-8Al-1Mo	5	107	55 to 70 hours
Ti-8Al-1Mo-1V	78	122	31 to 46 hours
Ti-8Al-2Mo	21	97	7 to 21 hours
Ti-4Al-2Mo-2V	1	97	Did not fail completely; small cracks noted at end of test - 27 days
Ti-8Al-2V	6	107	7 to 21 hours
Ti-6Al-4V STA		145	Approximately 24 hours

Fractography

The Ti-8Al and Ti-4Al alloys were selected as representative of two distinct types of cracking behavior, and fractured specimens of each alloy were examined by scanning-electron microscopy. Figure 15 shows the mixed fracture modes that have occurred in the Ti-8Al. Both transgranular fast fracture and intergranular attack have occurred. Figures 15a, 15b, and 15c are micrographs of the initiating edge of the fracture surface in this constant-deflection bent-beam specimen. It appears that the initial attack is intergranular and that fast transgranular fracture occurs when a critical stress intensity is reached at the root of the slowly growing intergranular crack. The river patterns in Figure 15c are characteristic of mechanical transgranular fracture. Two factors that could contribute to this initiation of fast fracture are: (1) the growth of the intergranular crack increases the stress-intensity factor and (2) the environment embrittles the metal at the crack tip, thus lowering the critical stress-intensity factor. Absorption of corrosion-produced hydrogen into the highly strained metal at the crack root could produce embrittlement. It would not be necessary to embrittle more than a small
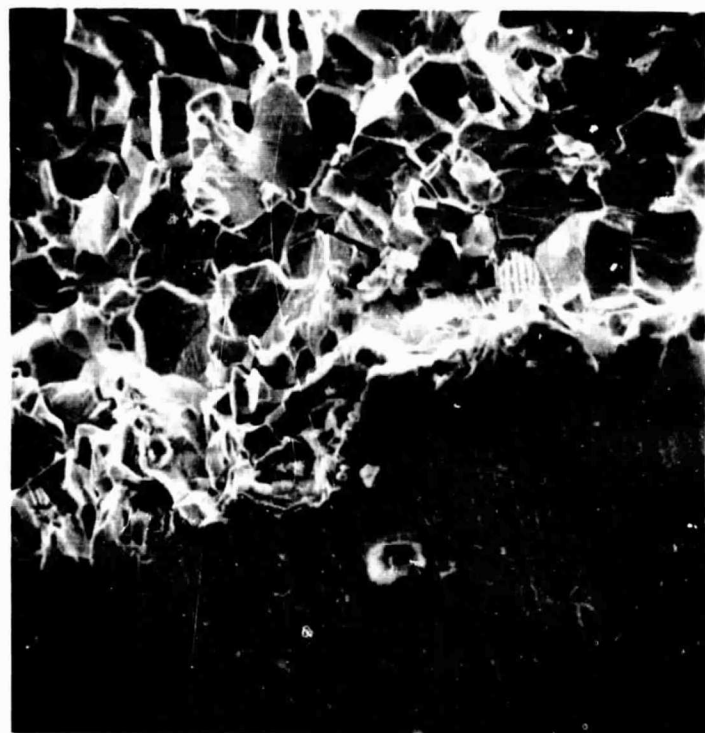
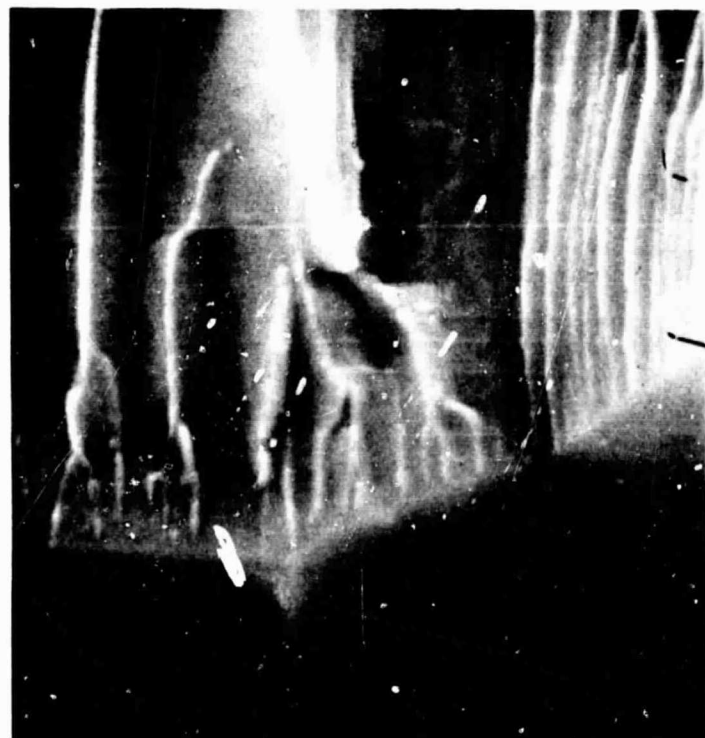200X   a.   SE166   1000X   b.   SE165

10,000X   c.   SE164   1000X   d.   SE167

FIGURE 15. SCANNING-ELECTRON MICROGRAPHS OF METHANOL
STRESS-CORROSION FRACTURES IN Ti-8Al

volume of metal at the crack tip because the propagation of a brittle fracture is strain-rate dependent as well as dependent on the stress-intensity factor.

In a constant-deflection bent-beam specimen, the stress-intensity factor should initially increase as the crack grows and then decrease beyond some point at which the remaining thickness of the specimen is too thin to produce the required stress. This fact is illustrated in this specimen by a change from fast transgranular fracture near the initiating edge to predominantly intergranular attack (Figure 15d) near the center of the specimen fracture surface. The many cracks perpendicular to the fracture face indicate that the intergranular attack may occur without an applied tensile stress.

Figures 16a and 16b show the definite intergranular nature of the methanol attack on the Ti-4Al alloy. Fast fracture did not occur in any of the experimental alloys containing 4 weight percent aluminum. The smoothness of the grain faces and the sharpness of the grain edges indicate that there was very little attack on the grain material. This behavior suggests that either dissolution of a continuous-grain-boundary material or the lowering of intergranular bond strengths has caused the grains to separate. Again, the presence of cracks perpendicular to the fracture surface indicates that applied stress may play a minor role in this process.
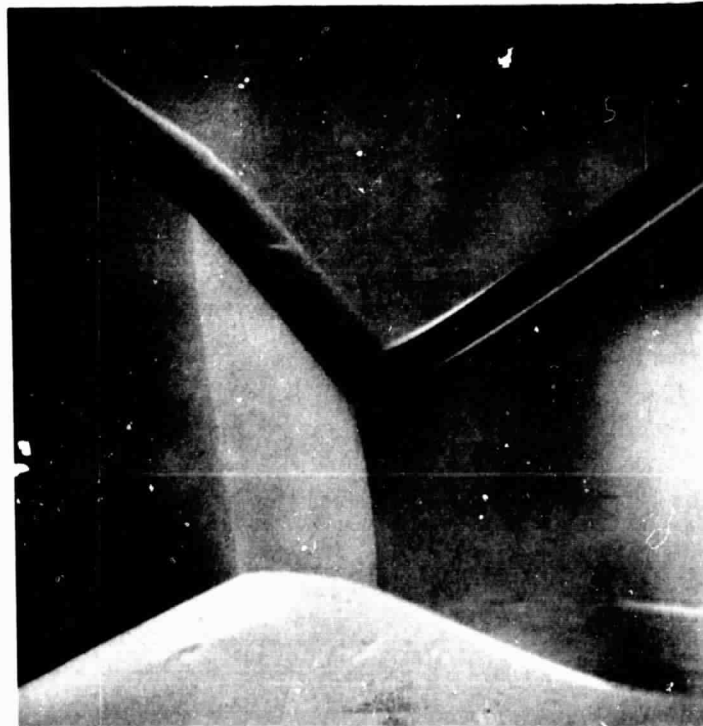

FIGURE 16. SCANNING-ELECTRON MICROGRAPHS OF METHANOL
STRESS-CORROSION FRACTURES IN Ti-4Al

Although a difference in strength levels between alloys containing 8 weight percent aluminum and alloys containing 4 weight percent aluminum could partially account for the observed differences in fracture modes, this correlation is not consistent. Seven out of eight of the alloys containing 4 weight percent aluminum are actually stronger than the Ti-6Al binary alloy. Thus it is concluded that the additional aluminum content interacts with the environment to produce a brittle fast fracture.

REFERENCES

(1) D. N. Fager and W. F. Spurr, Trans. ASM, 61, 283 (1968).

(2) G. Sanderson and J. C. Scully, Corros. Sci., 6, 541 (1966).

(3) D. T. Powell and J. C. Scully, "The Stress Corrosion Cracking of Alpha Titanium Alloys at Room Temperature", The Science Technology and Application of Titanium, R. I. Jaffee and N. E. Promisel (Eds.), Pergamon, Oxford (1969).

(4) T. R. Beck, "Electrochemical Mechanism in the Stress Corrosion Cracking of Titanium Alloys", loc. cit.

(5) S. P. Rideout, et al., "The Role of Moisture and Hydrogen in Hot-Salt Cracking of Titanium Alloys", paper presented at the Symposium on Stress-Corrosion Cracking, Columbus, Ohio, September, 1967.

JDB/FHH/PJM/WKB/RAW/DNW/RIJ:pa

END

DATE

FILMED

NOV 19 1969